Available online at www.sciencedirect.com
SCIENCE DIRECT®
Biochemical and Biophysical Research Communications 314 (2004) 1014–1020
BBRC
www.elsevier.com/locate/ybbrc

Direct measurement of Ca^{2+} concentration in the SR of living cardiac myocytes

Hiroki Kasai,[a,1] Atsushi Yao,[a,1] Tomomi Oyama,[b] Hiroshi Hasegawa,[b] Hiroshi Akazawa,[b] Haruhiro Toko,[b] Toshio Nagai,[b] Koichiro Kinugawa,[a] Osami Kohmoto,[c] Kei Maruyama,[d] Toshiyuki Takahashi,[a] Ryozo Nagai,[a] Atsushi Miyawaki,[e] and Issei Komuro[b,*]

[a] *Department of Cardiovascular Medicine, Graduate School of Medicine, University of Tokyo, Tokyo, Japan*
[b] *Department of Cardiovascular Science and Medicine, Chiba University Graduate School of Medicine, Chiba 260-8670, Japan*
[c] *The Second Department of Medicine, Saitama Medical School, Japan*
[d] *Department of Pharmacology, Saitama Medical School, Japan*
[e] *Laboratory for Cell Function and Dynamics, Advanced Technology Development Center, Brain Science Institute, The Institute of Physical and Chemical Science (RIKEN), Japan*

Received 17 December 2003

Abstract

Although abnormal sarcoplasmic reticulum (SR) Ca^{2+} handling may cause heart failure, there has been no method to directly measure Ca^{2+} concentration in SR ($[Ca^{2+}]_{SR}$) of living cardiomyocytes. We have measured $[Ca^{2+}]_{SR}$ by expressing novel fluorescent Ca^{2+} indicators *yellow cameleon* (YC) 2.1, YC3er, and YC4er in cultured neonatal rat cardiomyocytes. The distribution of YC2.1 was uniform in the cytoplasm, while that of YC3er/YC4er, containing the signal sequence which recruits them to SR, showed reticular pattern and was co-localized with SERCA2a. The treatment with caffeine reversibly decreased the emission ratio (R) in YC3er/YC4er-expressing myocytes, and the treatment with ryanodine and thapsigargin decreased R irreversibly. During the contraction–relaxation cycle, R was changed periodically in the YC2.1- and YC3er-expressing myocytes, but its direction of the change was opposite. These results suggest that YC3er/YC4er were specifically localized and functioned in SR as a $[Ca^{2+}]_{SR}$ indicator. This technique would be useful to understand the function of SR in failing myocardium.
© 2004 Elsevier Inc. All rights reserved.

Keywords: Sarcoplasmic reticulum; Fluorescent Ca^{2+} indicators; Yellow cameleon; Real-time monitoring; Cardiomyocyte; Caffeine; Thapsigargin; SERCA; Heart failure

Ca^{2+} is the primary regulator for the contraction–relaxation cycle in cardiac muscle, and the sarcoplasmic reticulum (SR) is a key organelle for physiological Ca^{2+} regulation in mammalian cardiomyocyte [1]. The accumulation of a small amount of Ca^{2+} in the diad junctions through the voltage dependent L-type Ca^{2+} channels induces a release of large amount of Ca^{2+} from SR through ryanodine receptors by the Ca^{2+}-induced Ca^{2+} release (CICR) mechanism, leading to myocardial contraction.

During relaxation, cytosolic Ca^{2+} concentration ($[Ca^{2+}]_{cyt}$) is decreased by sequestration into SR by the SR Ca^{2+}-ATPase (SERCA) or efflux from the cytosol by Na^+/Ca^{2+} exchanger (NCX) [2]. Dysfunction of the Ca^{2+} handling proteins of SR has recently been focused as one of the critical factors to cause heart failure [3–6]. Therefore, direct and precise measurement of the intra-SR Ca^{2+} concentration ($[Ca^{2+}]_{SR}$) in living cardiomyocyte is a prerequisite for understanding a molecular link between SR functions and heart failure. Since the kinetics of $[Ca^{2+}]_{SR}$ have been obtained from calculations based on many complicated assumptions such as Ca^{2+} buffering capacity of SR, SR volume, ionic strength, and performance of SERCA, and ryanodine receptors

* Corresponding author. Fax: +81-43-226-2557.
E-mail address: komuro-tky@umin.ac.jp (I. Komuro).
[1] These authors equally contributed to this work.

0006-291X/$ - see front matter © 2004 Elsevier Inc. All rights reserved.
doi:10.1016/j.bbrc.2003.12.189

[7–10], $[Ca^{2+}]_{SR}$ transient during every contraction–relaxation cycle has been only speculated. Recently, we have developed Ca^{2+} sensitive proteins yellow cameleons (YC) [11]. Among YC, YC3er, and 4er have the signal sequence which recruits them into the endoplasmic reticulum (ER), and reflect Ca^{2+} concentration in ER ($[Ca^{2+}]_{ER}$) in response to various stimulations in living non-muscle cells. So we have examined the real-time change of $[Ca^{2+}]_{SR}$ in living ventricular myocytes using YC3er and 4er.

Methods

This investigation conformed to the Guide for the Care and Use of Laboratory Animals (Washington, DC: Natl. Acad. Press, 1996).

Cell culture. Primary cultures of cardiac myocytes were prepared from ventricles of 1-day-old neonatal Wistar rats [12]. In brief, cells enzymatically dissociated from the ventricles were plated at a field density of 1×10^5 cells/cm^2 on 25×50 mm of collagen-coated coverslips in culture medium (Dulbecco's modified Eagle's medium with 10% fetal bovine serum). Twelve hours after seeding, the culture medium was changed to the medium with 0.5% fetal bovine serum.

Constructs of yellow cameleons. Plasmids containing YC2.1, YC3er, and YC4er were described previously [13]. YC3er and YC4er have a mutation of E104Q and E31Q, respectively, which is important for determination of the dissociation constant (K_d value). They also have the calreticulin leading sequence in the N terminus and the retention signal (KDEL) in the C terminus to introduce and detain these products in ER, respectively.

Transfection procedure of cameleon expression vectors. Twelve hours after plating the cells on coverslips, plasmid DNA of each cameleon was transfected using FuGENE6 (Roche, Basel, Switzerland). One microgram of DNA mixed with 3 μl of FuGENE6 reagent was added in the culture medium. The transfection efficiency of each experiment was ~5%, as determined by counting the number of cells which had significant emission of 530 nm-fluorescence excited by 420 ± 20 nm-light.

Staining of SR Ca^{2+}-ATPase (SERCA) 2a and actin filaments. After the transfection procedure, the cells were fixed with 4% paraformaldehyde-containing PBS and then permeated by 0.2% Triton X-contained PBS. For the immunostaining of SERCA2a, the cells were blocked with 5% fetal calf serum-contained PBS, incubated with affinity-purified monoclonal anti-SERCA2a antibodies (Affinity Bioreagents), and subsequently incubated with secondary fluorescein-conjugated anti-mouse IgG antibodies (CHEMICON, Temecula, USA). For the staining of the actin filaments, the permeated cells were stained with TRITC-labeled phalloidin (Sigma–Aldrich, St. Louis, USA).

Confocal images. Images were obtained using a confocal laser scanning microscopy system equipped with argon-laser and an acousto-optic tunable filter (Leica, Wetzlar, Germany). To obtain the fluorescence images from the cameleons and fluo-3, cells were excited at a wavelength of 488 nm and the emission light of 500–535 nm was acquired. The loading of fluo-3 was performed as described previously [14]. For the images of SERCA2a and actin filaments, cells were excited at 543 nm and then the emission light at 555–700 nm was acquired.

Measurement of $[Ca^{2+}]_{cyt}$ and $[Ca^{2+}]_{SR}$. The measurement of Ca^{2+} concentration was carried out with a modification of the method used for indo-1 [15]. In brief, cells were perfused with Hepes solution (126 mM NaCl, 4.4 mM KCl, 1.0 mM $MgCl_2$, 13 mM NaOH, 1.08 mM $CaCl_2$, 11 mM glucose, and 24 mM Hepes, adjusting pH to 7.4 at 25 °C) at a constant flow rate ($\geq$ 2 ml/min) in a heated chamber (24–6 °C) which was equipped on the stage of an inverted epifluorescence microscope (Nikon Diaphot). A myocyte expressing YC could be selected by the image of emission fluorescence passing through the dichroic mirror (DM455, Nikon), and non-myocytes having YCs fluorescence could be screened out because they did not contract in response to pacing stimulation. The myocyte within the field was then excited with the light from a 100 W mercury-arc lamp (Nikon) passing through a 420 ± 20 nm band pass filter (BV-2A, Nikon), and an emission fluorescence was detected simultaneously at 480 (BA, Nikon) and 530 nm (DF30, Omega) with a photomultiplier tube (PMT; model 1897 AH, Hamamatsu). The fluorescence of the optical field without YCs positive cells was measured as zero.

Data analysis. The emission signals from the YCs were digitized using a Digidata1200A analog-to-digital converter (Axon Instruments) and stored in a personal computer (Gateway). The data were analyzed with Axoscope1.0 (Axon Instruments) and Origin4.0 (Microcal) software.

Results

Expressing pattern of cameleons

YC2.1, YC3er, and YC4er were successfully expressed in cultured neonatal rat ventricular myocytes (Fig. 1). The protein of YC2.1 was localized in the cytosol in a homogeneous pattern except for the space probably occupied by intra-cellular organelles (Fig. 1A). As compared with the conventional Ca^{2+} sensitive dye fluo-3 (Fig. 1B), expression of YC2.1 was spared in the nucleus, suggesting that expression of YC2.1 is localized in the cytoplasm of cardiomyocytes. In contrast, YC3er showed fine reticular expression pattern around the nucleus and a ladder-like pattern in the peripheral region of cardiomyocytes (Fig. 1C). Immunocytochemisty using TRITC-labeled phalloidin revealed that the parallel lines of fine reticular region corresponded to the middle of actin filaments (I bands) (Figs. 1D–F), where there are diad junctions. Since these results suggest that YC3er is localized in SR, we examined the co-localization of YC3er and the SR protein SERCA2a. The expression pattern of YC3er was very similar to that of SERCA2a (Figs. 1G–I). The distribution of YC4er was also similar to that of YC3er (data not shown). Co-localization of YC3er and YC4er with SERCA2a at I bands suggests that YC3er and YC4er were located in SR membranes.

Ca^{2+} transient measured by cameleons

To evaluate the dynamics of intra-cellular Ca^{2+} transient, the emitted fluorescences of 480 and 530 nm from cameleons excited by 420 ± 20 nm-light were simultaneously recorded, and the ratio of 530- to 480 nm-intensity (R) was calculated. In the YC2.1-expressing myocyte, the end diastolic R was continuously raised by pacing (0.5 Hz) (Fig. 2a), and beat-to-beat oscillated R transient was seen during each contraction–relaxation cycle (Fig. 2a-A), which was quite similar to the signal monitored by use of conventional Ca^{2+} sensitive dyes

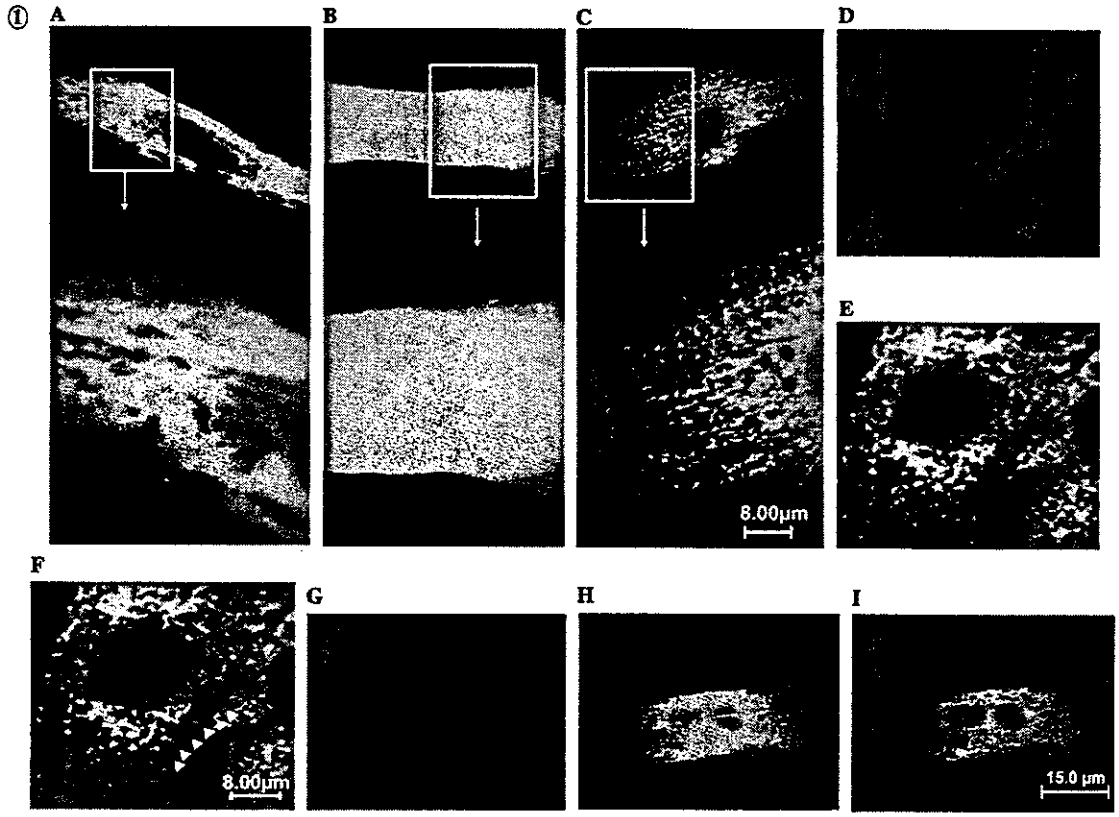
①
A
B
C
D
E
F
G
H
I
8.00μm
8.00μm
15.0 μm

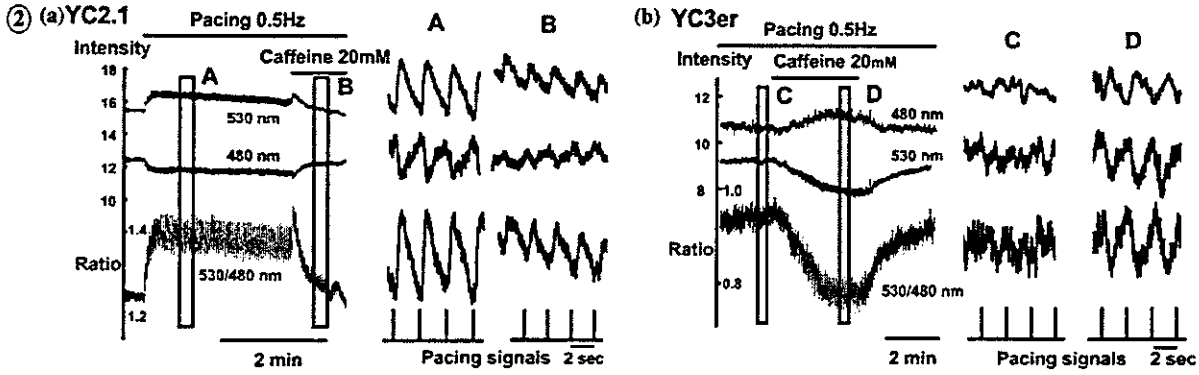
② (a)YC2.1
Pacing 0.5Hz
Intensity
Caffeine 20mM
A
B
530 nm
480 nm
Ratio
530/480 nm
2 min
Pacing signals 2 sec
(b) YC3er
Pacing 0.5Hz
Intensity
Caffeine 20mM
C
D
480 nm
530 nm
Ratio
530/480 nm
2 min
Pacing signals 2 sec

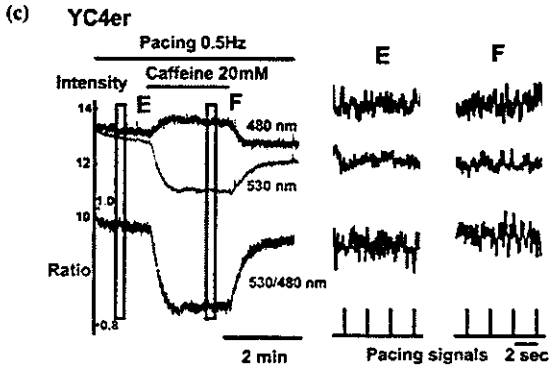
(c) YC4er
Pacing 0.5Hz
Intensity
Caffeine 20mM
E
F
480 nm
530 nm
Ratio
530/480 nm
2 min
Pacing signals 2 sec

Fig. 1. Confocal fluorescence images of YC2.1, YC3er-, and YC4er-expressing cells. (A) In the YC2.1-expressed myocyte, emitted fluorescence of 530 nm was uniform in the cytosol without any significant brighter spot. Fluorescence was spared in the nucleus. (B) In the fluo-3-loaded myocyte, the fluorescence of 530 nm was homogeneous in the cytosol and intra-cellular organelles with some brighter spots. (C) The image of the YC3er-expressed myocyte showed reticular pattern around the nucleus and a ladder-like pattern in the peripheral lesion of the myocyte. The YC4er-expressing myocyte (E) was simultaneously stained with TRITC-labeled phalloidin (D). The parallel lines (arrowheads) of YC4er-expressing region were located in the middle of the I bands (Merge, (F)). Note that the distance between the neighbored cross-sectional parallel lines was about 2 μm. Simultaneous detection of distribution of SERCA2a (G) and YC3er (H) was performed using confocal laser microscopy. The distribution of YC3er was overlapped with the expression pattern of SERCA2a (Merge, (I)).

Fig. 2. Ca^{2+}-dependent FRET signals from the YC2.1, YC3er-, and YC4er-expressing ventricular myocytes. In the YC2.1-expressing myocyte, the emission signals of 480 nm (black line) were decreased and the signals of 580 nm (red line) were increased by pacing stimulation (a). As a result, calculated *R* (blue line) was transiently increased during each contraction–relaxation cycle (A), and the rapid application of caffeine (20 mM) decreased both the diastolic and the amplitude of *R* (B) after transiently increasing the diastolic level of *R*. In the YC3er-expressed myocyte, *R* was reversibly decreased by caffeine (b). The beat-to-beat oscillation of the emission lights was observed after the caffeine-treatment (D) but not before the treatment (C). In the YC4er-expressed myocyte, *R* was decreased by caffeine-like in the YC3er-expressing myocyte (c), but the beat-to-beat oscillation was not observed with (F) or without (E) the treatment.

[16,17]. Treatment with 20 mM of caffeine initially and transiently increased the baseline (diastolic level) of *R*, resulting from an increase in the 530 nm-emission intensity and a decrease in the 480 nm-emission intensity, which was followed by a decrease in that of *R* with reduction in the amplitude of *R* transients (Fig. 2a-B). These results suggest that YC2.1 was localized in the cytosol and reflected a change in the cytosolic Ca^{2+} concentration ($[Ca^{2+}]_{cyt}$) during each contraction–relaxation cycle. In the YC3er-expressing myocyte, the emission of both 480 and 530 nm did not change synchronously by pacing stimulations (Fig. 2b-C). In contrast to YC2.1, the emission of 480 nm was increased and that of 530 nm was decreased by treatment with 20 mM of caffeine (Fig. 2b-D). A beat-to-beat periodical *R* transient was detected during the caffeine treatment and the phase of the *R* transient was completely inverted to that observed in the YC2.1-expressing myocyte (Figs. 2a-B and b-D). *R* was increased soon after pacing stimulation in the YC2.1 expressing myocyte (Fig. 2a), while *R* was peaked at pacing stimulation and decreased thereafter in the YC3er-expressing myocytes (Fig. 2b). In the YC4er-expressing myocyte, *R* was decreased by the treatment with caffeine (Fig. 2c), but periodical transient was not observed before and after caffeine treatment (Fig. 2c-E and F). Since caffeine induces efflux of Ca^{2+} from SR and we have confirmed that caffeine of this high concentration did not alter the emission signals from cardiac fibroblasts expressing YC3er or YC4er as well as HEK293 cells expressing YC2.1 (data not shown), the results of caffeine treatment suggest that change in the emission signals from YC3er and YC4er can be considered to be Ca^{2+}-dependent, that is, reflect the change in $[Ca^{2+}]_{SR}$.

Change of $[Ca^{2+}]_{SR}$

Next we examined the effects of Ca^{2+} modulating agents such as isoproterenol, thapsigargin, and ryanodine on *R*. Isoproterenol has been known to increase Ca^{2+} influx through L-type Ca^{2+} channels of sarcolemma, leading to an increase in large Ca^{2+} release from SR by the CICR mechanism. Isoproterenol also increases the pumping rate of SERCA2a by phosphorylating phospholamban through Gs protein-coupled protein kinase A activation. Addition of 100 nM isoproterenol increased *R* in the YC4er- and YC3er-expressing myocytes (Fig. 3A, data not shown). Thapsigargin has been widely used as an inhibitor for SERCA2a. As shown in Fig. 3B, 10 μM of thapsigargin decreased *R* in the YC4er-expressing myocyte, which was not reversed after removal of thapsigargin from the perfusate. Subsequent application of caffeine further decreased *R* and this reduction was reversed soon

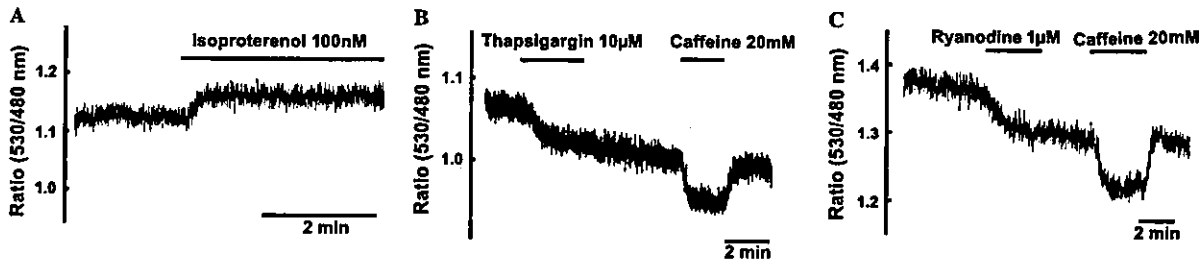

Fig. 3. Effects of isoproterenol, thapsigargin, and ryanodine on $[Ca^{2+}]_{SR}$. Treatment with 100 nM of isoproterenol increased *R* in the YC4er-expressed myocyte. (A) On the other hand, 10 μM of thapsigargin (B) or 1 μM of ryanodine (C) irreversibly decreased *R* in the YC4er-expressing myocyte and subsequent treatment with caffeine (20 mM) further decreased *R* reversibly.

after the end of caffeine treatment (Fig. 3B). Ryanodine at the concentration of 1 μM has been reported to increase the open probability of SR Ca^{2+} channel (ryanodine receptor) and consequently decrease $[Ca^{2+}]_{SR}$. As shown in Fig. 3C, the ryanodine treatment decreased R irreversibly and the subsequent application of caffeine further decreased R. Similar results were obtained in YC3er-expressing myocytes (data not shown).

Discussion

In the present study, we succeeded in specifically expressing YC2.1 in the cytoplasm and YC3er/4er in SR of living ventricular myocytes, and established the method for measuring $[Ca^{2+}]_{cyt}$ and $[Ca^{2+}]_{SR}$. The validity of the method for measuring $[Ca^{2+}]_{SR}$ was confirmed by the reverse directions of Ca^{2+} transient observed in YC2.1 expressing myocytes and YC3er-expressing myocytes during pacing and by the effects of isoproterenol, thapsigargin, and ryanodine on Ca^{2+} concentration in YC4er- and YC3er-expressing myocytes.

Intra-cellular distribution of cameleons

YC2.1 was expressed homogeneously in the cytoplasm, whereas YC3er and YC4er showed a characteristic expression pattern in ventricular myocytes. Expression of YC2.1 was spared in the nucleus or the intra-cellular organelles. Since molecular size of cameleons is relatively large (74 kDa), they could not get into those organellae. In contrast, conventional Ca^{2+} dyes can be taken by organellae such as mitochondria and Golgi apparatus as well as the nucleus. The cytosolic homogeneous pattern of YC2.1 also suggests that YC2.1 resides in the fluid space of the cytosol without accumulation or binding to hydrophobic proteins, which is consistent with results in non-muscle cells [11]. The specific localization and the uniform distribution give the priority to the YCs as a Ca^{2+} indicator as compared with conventional fluorescence indicators such as fura-2, indo-1, and fluo-3.

In mature ventricular myocytes, it has been reported that calsequestrin is a major protein to buffer Ca^{2+} in SR and is predominantly (60–70%) expressed in the terminal cisternae [18–20], while calreticulin composes a minor part [21]. YC3er and YC4er possess the leading sequence and the retention signal (KDEL) of calreticulin, which introduce and detain these cameleons in the ER of nonmyocytes [11]. YC4er was located in the middle of I-bands (Figs. 1D–F), suggesting that YC4er was expressed in the part of the terminal cisternae. Immunocytochemical analysis using anti-SERCA2a antibody indicated that YC3er and YC4er were localized in the same place as SERCA2a (Fig. 1H). These results suggest that YC3er and YC4er were expressed in terminal cisternae of SR.

$[Ca^{2+}]_{SR}$ transients

Although the relatively slow changes in $[Ca^{2+}]_{SR}$ were observed after several manipulations (Fig. 3), we could not observe the cyclic emission signals which were synchronized with beating in the YC3er/4er-expressing myocyte. Since treatment with caffeine unraveled beat-to-beat oscillated R in the YC3er-expressing cells, the limited speed of the Ca^{2+}-dependent conformational change of YC3er is not a major cause of irresponsiveness to pacing stimulations. The difference in beat-to-beat oscillation after caffeine treatment between YC3er and YC4er (Figs. 2b and c) suggests that the irresponsiveness might be at least in part due to dissociation constant (K_d). K_d of YC3er has been reported to be 4.4 μM at 25 °C [11,13]. In the earlier reports [10,22–24], $[Ca^{2+}]_{SR}$ has been reported to be 0.3–5 mM, the range of which is much higher than the K_d value for YC3er. Therefore, YC3er may be saturated with Ca^{2+} and it cannot follow the change in $[Ca^{2+}]_{SR}$. This interpretation seems to be reasonable, because the emission signals from YC3er actually showed beat-to-beat transients in response to pacing when Ca^{2+} in SR was reduced by caffeine. However, beat-to-beat signals were not detected from YC4er-expressing cardiomyocyte in response to pacing stimulation even after the caffeine treatment, suggesting that there are other reasons. The first possibility is that YC4er was expressed so much that YC4er itself buffered Ca^{2+} in SR as suggested previously [11,13], resulting in suppression of CICR and/or secondary modification of Ca^{2+} handling systems consisting of L-type Ca^{2+} channel, ryanodine receptors, the dyadic or triadic structure, and so on. In fact, the $[Ca^{2+}]_{cyt}$ transients were markedly reduced when the intra-SR buffering capacity was much increased by overexpression of calsequestrin, although the total Ca^{2+} content in SR was markedly increased [25,26]. The second possibility is that the intra-SR Ca^{2+} concentration may be out of the measurable range with YC3er and YC4er in neonatal rat ventricular myocytes. The Ca^{2+} titration curve for YC4er has been reported to be a biphasic sigmoid curve with rather linear relationship at 10^{-4}–10^{-2} M of Ca^{2+} concentration. This suggests that YC4er could not be used as a Ca^{2+} indicator in the range of Ca^{2+} concentrations below 10^{-4} M or above 10^{-2} M. On the other hand, the titration curve for YC3er has been reported to be well fitted with a single sigmoid curve with almost linear relationship between 10^{-7} and 10^{-5} M [11]. Therefore, resting $[Ca^{2+}]_{SR}$ might be 10^{-5}–10^{-4}. We could not achieve the calibration, because of deformation and rigor of cardiomyocytes when we increased $[Ca^{2+}]_{cyt}$ up to more than 10^{-2} M with ionomycin. Furthermore, both YC3er and YC4er did not

respond to high $[Ca^{2+}]_{SR}$ ($\geqslant 10^{-2}$ M) solution in the presence of ionomycin (data not shown), suggesting that the cell damage might affect the conditions of YC3er and YC4er in the SR. Further studies are necessary to establish precise calibration to use these cameleons for general measurements of $[Ca^{2+}]_{SR}$ in cardiac myocytes.

$[Ca^{2+}]_{SR}$ after addition of Ca^{2+} modulating agents

Although cameleons could not follow the rapid change of $[Ca^{2+}]_{SR}$, they could respond to the relatively slow and large change in $[Ca^{2+}]_{SR}$. Isoproterenol increased R in cardiac myocytes expressing YC4er and YC3er (Fig. 3A). Ten micromolars of thapsigargin has been widely used to diminish the pumping rate of SERCA2a, and has been reported to deplete SR Ca^{2+} content almost irreversibly because of its high affinity [27]. As shown in Fig. 3B, thapsigargin decreased R irreversibly. However, the subsequent application of caffeine further and reversibly decreased R, suggesting that the treatment with 10 μM of thapsigargin for 3 min is not enough to inhibit SERCA2a completely or to deplete Ca^{2+} storage in SR. Ryanodine at 1 μM has been thought to set the ryanodine receptor subconducting state [28], which likely accelerates the leak of Ca^{2+} from SR, and reduces $[Ca^{2+}]_{SR}$. As shown in Fig. 3C, ryanodine decreased R in the YC4er-expressing myocyte. The effect by subsequent application of caffeine was maintained, suggesting that ryanodine partially releases a part of Ca^{2+} in SR.

The effect of caffeine at the concentration of this range (20 mM) has been well recognized to set the ryanodine receptor subconducting state and prevent net SR Ca^{2+} reuptake [29], both of which result in Ca^{2+} release from SR and the depletion of releasable Ca^{2+} in SR. Therefore, the beat-to-beat $[Ca^{2+}]_{cyt}$ oscillation induced by pacing in the presence of caffeine has been thought to be mediated by Ca^{2+} influx through L-type Ca^{2+} channels and reverse phase of NCX. In this study, however, CICR was detectable by cameleons even after the caffeine treatment. Caffeine has been reported to inhibit phosphodiesterases to increase cAMP, thereby activating SERCA as well as further increasing I_{Ca} through protein kinase A-dependent mechanism, both of which may contribute to maintaining the amount of releasable Ca^{2+} in SR. Reconsideration may be necessary for the effects of caffeine on Ca^{2+} regulation in cardiomyocytes, although it is not ruled out that difference in species, age, and experimental conditions might contribute to this intricate effect of caffeine.

In conclusion, we for the first time succeeded in monitoring the real-time changes of $[Ca^{2+}]_{SR}$ in living ventricular myocytes expressing novel Ca^{2+} indicators, YC3er and YC4er. We also examined the effects of drugs which modify the function of SR Ca^{2+} handling proteins such as SERCA2a and ryanodine receptors. Although the calibration of emission signals to Ca^{2+} concentration has not be established, this technique is useful and applicable to evaluate the $[Ca^{2+}]_{SR}$ in cardiomyocytes of pathological and various pathophysiological conditions.

Acknowledgments

This work was partly supported by a Grant-in-Aid for Scientific Research on Priority Areas from the Ministry of Education, Culture, Sports, Science and Technology of Japan, Japan Heart Foundation, Takeda Medical Research Foundation, Uehara Memorial Foundation, and Grant-in-Aid of Japan Medical Association, The Kato Memorial Trust for Nambyo Research, and Takeda Science Foundation. We thank Dr. Makoto Endo and Dr. William. H. Barry for their kind suggestions on the experimental protocols and the results in this study.

References

[1] D.M. Bers, Cardiac excitation–contraction coupling, Nature 415 (2002) 198–205.
[2] W.H. Barry, J.H. Bridge, Intracellular calcium homeostasis in cardiac myocytes, Circulation 87 (1993) 1806–1815.
[3] R. Studer, H. Reinecke, J. Bilger, T. Eschenhagen, M. Bohm, G. Hasenfuss, H. Just, J. Holtz, H. Drexler, Gene expression of the cardiac Na(+)–Ca^{2+} exchanger in end-stage human heart failure, Circ. Res. 75 (1994) 443–453.
[4] M. Meyer, W. Schillinger, B. Pieske, C. Holubarsch, C. Heilmann, H. Posival, G. Kuwajima, K. Mikoshiba, H. Just, G. Hasenfuss, Alterations of sarcoplasmic reticulum proteins in failing human dilated cardiomyopathy, Circulation 92 (1995) 778–784.
[5] S. Minamisawa, M. Hoshijima, G. Chu, C.A. Ward, K. Frank, Y. Gu, M.E. Martone, Y. Wang, J. Ross Jr., E.G. Kranias, W.R. Giles, K.R. Chien, Chronic phospholamban–sarcoplasmic reticulum calcium ATPase interaction is the critical calcium cycling defect in dilated cardiomyopathy, Cell 99 (1999) 313–322.
[6] S.O. Marx, S. Reiken, Y. Hisamatsu, T. Jayaraman, D. Burkhoff, N. Rosemblit, A.R. Marks, PKA phosphorylation dissociates FKBP12.6 from the calcium release channel (ryanodine receptor): defective regulation in failing hearts, Cell 101 (2000) 365–376.
[7] J.W. Bassani, R.A. Bassani, D.M. Bers, Twitch-dependent SR Ca accumulation and release in rabbit ventricular myocytes, Am. J. Physiol. 265 (1993) C533–C540.
[8] D.A. Eisner, H.S. Choi, M.E. Diaz, S.C. O'Neill, A.W. Trafford, Integrative analysis of calcium cycling in cardiac muscle, Circ. Res. 87 (2000) 1087–1194.
[9] A.W. Trafford, M.E. Diaz, D.A. Eisner, A novel, rapid and reversible method to measure Ca buffering and time-course of total sarcoplasmic reticulum Ca content in cardiac ventricular myocytes, Pflugers Arch. 437 (1999) 501–503.
[10] W. Hasselbach, H. Oetliker, Energetics and electrogenicity of the sarcoplasmic reticulum calcium pump, Annu. Rev. Physiol. 45 (1983) 325–339.
[11] A. Miyawaki, J. Llopis, R. Heim, J.M. McCaffery, J.A. Adams, M. Ikura, R.Y. Tsien, Fluorescent indicators for Ca^{2+} based on green fluorescent proteins and calmodulin, Nature 388 (1997) 882–887.
[12] P. Simpson, A. McGrath, S. Savion, Myocyte hypertrophy in neonatal rat heart cultures and its regulation by serum and by catecholamines, Circ. Res. 51 (1982) 787–801.
[13] A. Miyawaki, O. Griesbeck, R. Heim, R.Y. Tsien, Dynamic and quantitative Ca^{2+} measurements using improved cameleons, Proc. Natl. Acad. Sci. USA 96 (1999) 2135–2140.

[14] A. Yao, H. Matsui, K.W. Spitzer, J.H. Bridge, W.H. Barry, Sarcoplasmic reticulum and Na^+/Ca^{2+} exchanger function during early and late relaxation in ventricular myocytes, Am. J. Physiol. 273 (1997) H2765–H2773.

[15] A. Yao, T. Takahashi, T. Aoyagi, K. Kinugawa, O. Kohmoto, S. Sugiura, T. Serizawa, Immediate-early gene induction and MAP kinase activation during recovery from metabolic inhibition in cultured cardiac myocytes, J. Clin. Invest. 96 (1995) 69–77.

[16] K. Kinugawa, T. Takahashi, O. Kohmoto, A. Yao, H. Ikenouchi, T. Serizawa, Ca(2+)-growth coupling in angiotensin II-induced hypertrophy in cultured rat cardiac cells, Cardiovasc. Res. 30 (1995) 419–431.

[17] Y. Zou, A. Yao, W. Zhu, S. Kudoh, Y. Hiroi, M. Shimoyama, H. Uozumi, O. Kohmoto, T. Takahashi, F. Shibasaki, R. Nagai, Y. Yazaki, I. Komuro, Isoproterenol activates extracellular signal-regulated protein kinases in cardiomyocytes through calcineurin, Circulation 104 (2001) 102–108.

[18] A.O. Jorgensen, K.P. Campbell, Evidence for the presence of calsequestrin in two structurally different regions of myocardial sarcoplasmic reticulum, J. Cell Biol. 98 (1984) 1597–1602.

[19] A.O. Jorgensen, A.C. Shen, W. Arnold, P.S. McPherson, K.P. Campbell, The Ca^{2+}-release channel/ryanodine receptor is localized in junctional and corbular sarcoplasmic reticulum in cardiac muscle, J Cell Biol. 120 (1993) 969–980.

[20] A.O. Jorgensen, A.C. Shen, K.P. Campbell, Ultrastructural localization of calsequestrin in adult rat atrial and ventricular muscle cells, J. Cell Biol. 101 (1985) 257–268.

[21] T.J. Ostwald, D.H. MacLennan, Isolation of a high affinity calcium-binding protein from sarcoplasmic reticulum, J. Biol. Chem. 249 (1974) 974–979.

[22] T. Kodama, Thermodynamic analysis of muscle ATPase mechanisms, Physiol. Rev. 65 (1985) 467–551.

[23] C. Tanford, Mechanism of free energy coupling in active transport, Annu. Rev. Biochem. 52 (1983) 379–409.

[24] W. Chen, C. Steenbergen, L.A. Levy, J. Vance, R.E. London, E. Murphy, Measurement of free Ca^{2+} in sarcoplasmic reticulum in perfused rabbit heart loaded with 1,2-bis(2-amino-5,6-difluorophenoxy)ethane-*N*,*N*,*N*′,*N*′-tetraacetic acid by 19F NMR, J. Biol. Chem. 271 (1996) 7398–7403.

[25] L.R. Jones, Y.J. Suzuki, W. Wang, Y.M. Kobayashi, V. Ramesh, C. Franzini-Armstrong, L. Cleemann, M. Morad, Regulation of Ca^{2+} signaling in transgenic mouse cardiac myocytes overexpressing calsequestrin, J. Clin. Invest. 101 (1998) 1385–1393.

[26] Y. Sato, D.G. Ferguson, H. Sako, G.W. Dorn 2nd, V.J. Kadambi, A. Yatani, B.D. Hoit, R.A. Walsh, E.G. Kranias, Cardiac-specific overexpression of mouse cardiac calsequestrin is associated with depressed cardiovascular function and hypertrophy in transgenic mice, J. Biol. Chem. 273 (1998) 28470–28477.

[27] L. Hove-Madsen, D.M. Bers, Sarcoplasmic reticulum Ca^{2+} uptake and thapsigargin sensitivity in permeabilized rabbit and rat ventricular myocytes, Circ. Res. 73 (1993) 820–828.

[28] J.L. Sutko, J.A. Airey, W. Welch, L. Ruest, The pharmacology of ryanodine and related compounds, Pharmacol. Rev. 49 (1997) 53–98.

[29] R.A. Bassani, J.W. Bassani, D.M. Bers, Mitochondrial and sarcolemmal Ca^{2+} transport reduce $[Ca^{2+}]i$ during caffeine contractures in rabbit cardiac myocytes, J. Physiol. 453 (1992) 591–608.

Diabetologia (2004) 47:794–805
DOI 10.1007/s00125-004-1391-x

Diabetologia

Oxidative stress induces insulin resistance by activating the nuclear factor-κB pathway and disrupting normal subcellular distribution of phosphatidylinositol 3-kinase

T. Ogihara[1,2] · T. Asano[1] · H. Katagiri[2] · H. Sakoda[3] · M. Anai[3] · N. Shojima[1] · H. Ono[3] · M. Fujishiro[1] · A. Kushiyama[1] · Y. Fukushima[1] · M. Kikuchi[3] · N. Noguchi[4] · H. Aburatani[4] · Y. Gotoh[5] · I. Komuro[6] · T. Fujita[1]

[1] Department of Internal Medicine, Graduate School of Medicine, University of Tokyo, Tokyo, Japan
[2] Division of Advanced Therapeutics for Metabolic Diseases, Center for Translational and Advanced Animal Research on Human Diseases, Tohoku University Graduate School of Medicine, Sendai, Japan
[3] The Institute for Adult Diseases, Asahi Life Foundation, Tokyo, Japan
[4] Research Center for Advanced Science and Technology, University of Tokyo, Tokyo, Japan
[5] Department of Molecular Biology, Institute of Molecular and Cellular Biosciences, University of Tokyo, Tokyo, Japan
[6] Department of Cardiovascular Science and Medicine, Chiba University Graduate School of Medicine, Chiba, Japan

Abstract

Aims/hypothesis. Oxidative stress is associated with diabetes, hypertension and atherosclerosis. Insulin resistance is implicated in the development of these disorders. We tested the hypothesis that oxidative stress induces insulin resistance in rats, and endeavoured to identify mechanisms linking the two.
Methods. Buthionine sulfoximine (BSO), an inhibitor of glutathione synthase, was administered to Sprague-Dawley rats and 3T3-L1 adipocytes. Glucose metabolism and insulin signalling both in vivo and in 3T3-L1 adipocytes were examined. In 3T3-L1 adipocytes, the effects of overexpression of a dominant negative mutant of inhibitory κB (IκB), one role of which is to block oxidative-stress-induced nuclear factor (NF)-κB activation, were investigated.
Results. In rats given BSO for 2 weeks, the plasma lipid hydroperoxide level doubled, indicating increased oxidative stress. A hyperinsulinaemic-euglycaemic clamp study and a glucose transport assay using isolated muscle and adipocytes revealed insulin resistance in BSO-treated rats. BSO treatment also impaired insulin-induced glucose uptake and GLUT4 translocation in 3T3-L1 adipocytes. In BSO-treated rat muscle, adipose tissue and 3T3-L1 adipocytes, insulin-induced IRS-1 phosphorylation in the low-density microsome (LDM) fraction was specifically decreased, while that in whole cell lysates was not altered, and subsequent translocation of phosphatidylinositol (PI) 3-kinase from the cytosol and the LDM fraction was disrupted. BSO-induced impairments of insulin action and insulin signalling were reversed by overexpressing the dominant negative mutant of IκB, thereby suppressing NF-κB activation.
Conclusions/interpretation. Oxidative stress induces insulin resistance by impairing IRS-1 phosphorylation and PI 3-kinase activation in the LDM fraction, and NF-κB activation is likely to be involved in this process.

Keywords Buthionine sulfoximine · Glutathione · Hyperinsulinaemic-euglycaemic clamp · Inhibitory κB · Insulin resistance · IRS · Nuclear factor-κB · Oxidative stress · Phosphatidylinositol 3-kinase

Received: 20 October 2003 / Accepted: 26 January 2004
Published online: 1 May 2004
© Springer-Verlag 2004

T. Asano (✉)
Department of Internal Medicine, Graduate School of Medicine, University of Tokyo, Tokyo 113-8655, Japan
E-mail: asano-tky@umin.ac.jp
Tel.: +81-3-38153411 ext. 33133, Fax: +81-3-58031874

Present address:
T. Asano
Department of Physiological Chemistry and Metabolism, Graduate School of Medicine, University of Tokyo, Tokyo 113-8655, Japan

Introduction

Oxidative stress represents an imbalance between production of reactive oxygen species and the antioxidant defence system [1]. Oxidative stress is widely recognised as being associated with various disorders including diabetes, hypertension and atherosclerosis. In-

Abbreviations: BSO, buthionine sulfoximine · GMSA, gel mobility shift assay · IκB, inhibitory κB · IKK, IκB kinase · LDM, low-density microsome · NF-κB, nuclear factor-κB · PI, phosphatidylinositol

sulin resistance is a common feature of these disorders [2, 3]. Indeed, in diabetic people and in animal models of diabetes, the plasma free radical concentration is increased [4, 5] and antioxidant defences are diminished [6, 7]. It has also been suggested that antioxidant agents such as vitamin C [8] and E [9] improve insulin action in diabetic subjects.

Angiotensin II reportedly induces free radical production and increases plasma oxidative stress [10]. In our previous study, we showed continuous infusion of angiotensin II to induce insulin resistance with increased oxidative stress in rats, while the spin trap agent tempol [11], which works as a superoxide dismutase mimetic, decreases oxidative stress and improves insulin resistance in these rats [12]. A similar coexistence of oxidative stress and insulin resistance, as well as recovery with tempol administration was observed in adrenomedullin-deficient mice [13]. These previous reports strongly suggest a close relationship between oxidative stress and insulin resistance. Thus, we attempted to elucidate the molecular mechanisms underlying insulin resistance and oxidative stress.

In this study, to increase oxidative stress in vivo, we utilised a selective inhibitor of γ-glutamylcysteine synthetase, i.e. an inhibitor of glutathione synthase, buthionine sulfoximine (BSO). Glutathione is one of the major components of the antioxidant defence system, such that BSO administration increases oxidative stress by reducing the tissue glutathione level [14]. Although BSO does not have toxic effects in animals [14], BSO-treated rats were previously shown to exhibit glucose intolerance [15] and hypertension [16]. In the current study, we examined the effect of BSO treatment on insulin resistance in rats and 3T3-L1 adipocytes. We investigated the molecular mechanisms underlying BSO-induced insulin resistance, focusing on the subcellular distribution of phosphatidylinositol (PI) 3-kinase. Finally, we examined the involvement of the nuclear factor (NF)-κB pathway in BSO-induced insulin resistance and insulin signalling impairment.

Materials and methods

Materials. Affinity-purified antibodies against IRS-1 and GLUT4 were prepared as previously described [17]. Antibodies against phosphotyrosine, the p85 subunit of PI 3-kinase, and inhibitory κB (IκB) were purchased from Upstate Biotechnology (Milton Keynes, UK). TNF-α and buthionine-[S, R]-sulfoximine (BSO) were purchased from Sigma-Aldrich (St. Louis, Mo., USA).

Animals. Seven-week-old male Sprague-Dawley rats (Tokyo Experimental Animals, Tokyo, Japan) were fed a standard rodent diet with or without water containing 30 mmol/l BSO for 14 days [16]. The animal care was in accordance with the policies of the University of Tokyo, and the "Principles of laboratory animal care" (NIH publication no. 85-23, revised 1985) were followed.

Measurements. Cholesteryl ester hydroperoxides were analysed by HPLC, with 234 nm UV detection and post-column chemiluminescence detection on an LC-8 column (Supelco, 4×250 mm, 5-μm particles; Sigma-Aldrich) and methanol/tert-butyl alcohol (95/5 vol) as the eluent, as reported previously but with slight modification [18]. In brief, plasma was extracted with 10 volumes of methanol and 50 volumes of hexane. The hexane phase was removed, dried under N_2 gas and redissolved in an eluent for HPLC injection. Liver glutathione content was measured spectrophotometrically using a glutathione reductase recycling assay, as described previously [19].

Hyperinsulinaemic-euglycaemic clamp study. Rats fasted overnight were anaesthetised by intraperitoneal injection of pentobarbital sodium (60 mg/kg body weight) and the left jugular and femoral veins were catheterised for blood sampling and infusion respectively. Hyperinsulinaemic-euglycaemic clamp analysis was performed as described previously [17]. The glucose utilisation rate, hepatic glucose production and an estimate of muscle glucose uptake during the clamp (defined as the glucose metabolic index) were calculated as previously described [20].

Glucose uptake into isolated soleus muscle. Rats fasted overnight were anaesthetised and soleus muscles were dissected out and rapidly cut into 20–40 mg strips. The rats were then killed by intracardiac injection of pentobarbital. Isolated soleus muscle was incubated for 20 min with or without 1.44×10^{-8} mol/l human insulin (this concentration is equivalent to 2 mU/ml), as described previously [17]. 2-Deoxy glucose uptake into the isolated soleus muscle strips was measured using 2-deoxy-D-[^{3}H]glucose and [^{14}C]manitol as described previously [21].

Preparation of rat adipocytes and measurement of glucose uptake. Isolated rat adipocytes were prepared from epididymal adipose tissue harvested from fasted rats using the collagenase method [22], and 2-deoxy glucose uptake was then assayed as previously described [23].

Adenovirus-mediated gene transfer to 3T3-L1 adipocytes. 3T3-L1 fibroblasts were maintained in DMEM supplemented with 10% donor calf serum and differentiated into adipocytes as previously described [24]. The dominant negative mutant of IκB-α, in which serine residues 32 and 36 were substituted with alanine, was kindly provided by Dr R. Gaynor (University of Texas Southwestern Medical Center at Dallas, Tex., USA). To obtain recombinant adenovirus, pAdeno-X was ligated with cDNA encoding *Escherichia coli* lacZ and dominant negative IκB according to the manufacturer's instructions for the Adeno-X Expression System (Clontech, Palo Alto, Calif., USA). Infection of 3T3-L1 adipocytes with the adenovirus was carried out as described previously [25]. Recombinant adenoviruses were applied at a multiplicity of infection of approximately 200–300 pfu/cell and 3T3-L1 adipocytes infected with lacZ virus were used as a control.

Gel mobility shift assay. Nuclear protein extracts from 3T3-L1 adipocytes were prepared using NE-PER nuclear and cytoplasmic extraction reagents (Pierce Biotechnology, Rockford, Ill., USA) according to the manufacturer's instructions and used for gel mobility shift assay (GMSA). Briefly, 3T3-L1 adipocytes were homogenised in 1 ml of PBS and centrifuged for 10 min at 500 × *g* at 4 °C. After removing the supernatant, the pellet was resuspended in 500 μl of Cytoplasmic Extraction Reagent I buffer containing protease inhibitors (1 600 mol/l benzamidine, 0.3 mmol/l aprotinin, 4.2 mol/l leupeptin, 0.2 mol/l phenylmethylsulfonyl fluoride), and was incubated

on ice for 10 min. Then, 27.5 µl of Cytoplasmic Extraction Reagent II buffer were added to the sample, which was vortexed and centrifuged at 16 000 × *g* for 5 min. The resultant pellet was resuspended in 250 µl of NER buffer, vortexed every 10 minutes for 40 min and then centrifuged at 16 000 × *g* for 10 min. The supernatant containing nuclear proteins was stored at −80 °C. For the GMSA, 10 µg of nuclear proteins were incubated in binding buffer with 3.5 pmol of double-stranded DNA oligonucleotide containing an NF-κB consensus-binding sequence labelled with [^{32}P]-ATP using T4 polynucleotide kinase for 30 min at 37 °C. For supershift analyses, monoclonal antibody against NF-κB p65 was separately pre-incubated with nuclear extracts at 4 °C for 20 min in a total volume of 16 µl of binding buffer, followed by incubation with 8 µl of ^{32}P-labelled oligonucleotide probe with and without cold oligonucleotide probe at 4 °C for 20 min using a Nushift Kit (Geneka Biotechnology, Carlsbad, Calif., USA). Protein-DNA complexes were separated from the unbound DNA probe by electrophoresis through 5% polyacrylamide gels containing 1× Tris-glycine-EDTA buffer. The gel was dried and exposed to BAS2000 (Fujifilm, Tokyo, Japan).

Glucose uptake into 3T3-L1 adipocytes. 3T3-L1 adipocytes plated in 24-well culture dishes were serum starved for 3 h in DMEM containing 0.2% bovine serum albumin, after which they were incubated in Krebs–Ringer phosphate buffer for an additional 45 min, prior to incubation with or without 10^{-6} or 10^{-7} mol/l insulin for 15 min. The assay was initiated by adding 2-deoxy-D-[^{3}H]glucose (1.85×10^{7} Bq/sample, 0.1 mmol) and was terminated 4 min later by washing the cells once with ice-cold Krebs–Ringer phosphate buffer containing 0.3 mmol/l phloretin and then twice with ice-cold Krebs–Ringer phosphate buffer. The cells were then solubilised in 0.1% SDS, and the incorporated radioactivity was determined by scintillation counting [26].

Subcellular fractionation. 3T3-L1 adipocytes were serum starved for 3 h and incubated with or without 10^{-6} mol/l insulin for 15 min. Cells were fractionated as described previously [27]. Briefly, 3T3-L1 adipocytes were resuspended in HES buffer (255 mmol/l sucrose, 20 mmol/l HEPES [pH 7.4], 1 mmol/l EDTA), homogenised and subjected to differential centrifugation. The supernatants from the following spins were serially removed and pelleted in a Ti70 rotor as follows: 19 000 × *g* (20 min), 41 000 × *g* (20 min) and 180 000 × *g* (75 min). The first 19 000 × *g* pellet was resuspended, loaded onto a sucrose cushion (1.12 mol/l sucrose, 20 mmol/l HEPES [pH 7.4], 1 mmol/l EDTA) and isolated from the interface yielding the plasma membrane fraction as the pellet of a 41 000 × *g* spin (20 min). The last 180 000 × *g* pellet corresponded to the low-density microsome (LDM) fraction. Subcellular fractionation and measurement of GLUT4 translocation in isolated skeletal muscle and adipocytes from rats were described previously [12]. After resuspension of the pellets in solubilisation buffer, 20 µg of each fraction were loaded for western blotting. Proteins in the plasma membrane and LDM fractions were separated by SDS-PAGE, transferred to a polyvinylidene fluoride membrane, immunoblotted with anti-GLUT4, anti-IRS-1 or anti-p85 antibodies, and reacted with enhanced chemiluminescence reagent (Amersham Biosciences, Uppsala, Sweden) or subject to immunoprecipitation and PI 3-kinase assay of the immunoprecipitates as previously described [17].

Immunoprecipitation and immunoblotting. In rat experiments, rats fasted overnight were anaesthetised, and within 10–15 min the abdominal cavity was opened, the portal vein exposed, and 16 ml/kg body weight of normal saline (0.9% NaCl), with or without 10^{-5} mol/l human insulin, were injected. After 60 s, hindlimb muscles were removed and immediately homogenised as described previously [28]. In 3T3-L1 experiments, 3T3-L1 adipocytes were serum-starved for 18 h, pre-incubated with or without 80 µmol/l BSO for 18 h, then stimulated with or without 10^{-6} mol/l insulin for 15 min. The cells were then washed and lysed with lysis buffer as described previously [29]. After centrifugation, the resultant supernatants were used for immunoprecipitation or immunoblotting as described previously [28]. Proteins were visualised with enhanced chemiluminescence and band intensities were quantified with a Molecular Imager GS-525 using Imaging Screen-CH (Bio-Rad Laboratories, Hercules, Calif., USA). In some experiments, 3T3-L1 cells were incubated with 5.8 pmol/l (equivalent to 10 ng/dl) TNF-α or 80 µmol/l BSO for 18 h, lysed and immunoblotted with anti-IκB antibody.

Phosphatidylinositol 3-kinase activity. After preparing tissue samples as above, IRS-1 was immunoprecipitated, and PI 3-kinase activity in the immunoprecipitates was assayed as previously described [17].

Statistical analysis. Data are expressed as means ± SE. Comparisons between the two groups were made using unpaired *t* tests. We considered *p* values of less than 0.05 to be statistically significant.

Results

Characterisation of rats studied. Although food intakes were similar in the two groups, the BSO-treated rats had lower body weights than control rats (Table 1). Individual water consumptions did not differ between the two. Systolic and diastolic blood pressures were similar in the two groups of rats. Fasting blood glucose and plasma insulin levels in BSO rats were also similar to those of control rats. Although fasting insulin levels were not elevated in BSO-treated rats as compared with those of controls, we found that

Table 1. Characterisation of BSO-treated rats

	Control	BSO
Body weight (g)	320.0±8.7	284±4.1*
Food intake (g/day)	20.2±2.4	21.2±2.3
Water intake (ml/day)	38.2±1.8	36.8±3.2
Systolic BP (mm Hg)	113.5±4.4	120.7±3.9
Diastolic BP (mm Hg)	83.4±4.4	87.8±1.4
Fasting blood glucose (mmol/l)	6.12±0.32	6.32±0.24
Randomly fed blood glucose (mmol/l)	8.37±0.24	8.44±0.17
Fasting plasma insulin (pmol/l)	109±16	112±3
Randomly fed plasma insulin (pmol/l)	188±17	367±3*
Glutathione content of liver (µmol/g tissue)	3.2±0.3	1.1±0.4*
Plasma cholesteryl ester hydroperoxide (mmol/l)	1.38±0.3	2.72±0.3*

Data are means ± SE; rats in each group, $n=6$; * $p<0.05$ compared with controls

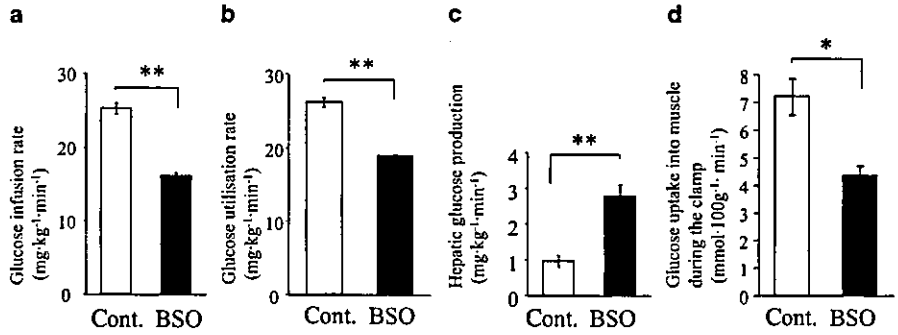

Fig. 1. A hyperinsulinaemic-euglycaemic clamp study. Rats were anaesthetised by intraperitoneal injection of pentobarbital sodium and the left jugular and femoral veins were catheterised for blood sampling and infusion respectively. Hyperinsulinaemic-euglycaemic clamp analysis was performed as described previously [17]. The glucose infusion rate (**a**), glucose utilisation rate (**b**), hepatic glucose production (**c**) and muscle glucose uptake during the clamp (defined as the glucose metabolic index; **d**) were estimated from hyperinsulinaemic-euglycaemic clamp data. * $p<0.05$, ** $p<0.01$ compared with the control. Bars represent the means ± SE of results from four to five rats. Cont. indicates control Sprague-Dawley rats. BSO indicates rats fed a standard rodent diet with water containing 30 mmol/l BSO for 12 days

among well-fed animals, insulin levels in BSO-treated rats were significantly higher than those in controls. To determine the effect of BSO as a glutathione synthase inhibitor, hepatic glutathione content was measured, because glutathione is most abundant in the liver. The glutathione level was significantly lower, by 34%, in the livers of BSO-treated rats than in those of controls. The cholesteryl ester hydroperoxide level in BSO-treated rat plasma was double that in control rats, suggesting that oxidative stress is increased in BSO-treated rats.

Hyperinsulinaemic-euglycaemic clamp study. Whole-body insulin sensitivity was evaluated using a hyperinsulinaemic-euglycaemic clamp technique. Compared with controls, the glucose infusion rate was decreased by 36.2% and the glucose utilisation rate by 27.6% during submaximal insulin infusion in BSO-treated rats (Figs. 1a, b). In addition, hepatic glucose production was increased by 29.3% in BSO-treated rats, suggesting impairment of the ability of insulin to suppress hepatic glucose production (Fig. 1c). Glucose uptake into skeletal muscle during the clamp was decreased by 39.4% in BSO-treated rats (Fig. 1d). These results suggest that BSO treatment induces insulin resistance both systemically and in skeletal muscle and liver.

Insulin-induced glucose uptake and GLUT4 translocation in BSO-treated rat skeletal muscle and adipocytes. In BSO-treated rats, insulin-induced glucose uptakes into isolated soleus muscle and adipocytes were reduced by 21.4% and 47.8% respectively as compared with the control levels (Figs. 2a, c). Subsequent western blot analysis showed the GLUT4 contents of skeletal muscle and adipocytes to be similar in the two groups (Figs. 2b, d, upper panels), indicating that the impairment of insulin-induced glucose uptake in these tissues from BSO-treated rats was not due to reduced expression of GLUT4 proteins. However, insulin-induced GLUT4 translocation, as assessed by the appearance of GLUT4 in the plasma membrane fraction of skeletal muscle and adipose tissue, was decreased in BSO-treated rats (Figs. 2b, d, lower panels). Microscopic analysis revealed adipocytes from BSO-treated rats to be small, which is consistent with the low body weights of these rats (Fig. 2e), suggesting that insulin resistance in BSO-treated rats is not attributable to adipocyte enlargement.

Impairment of insulin signalling in BSO-treated rat skeletal muscle and adipocytes. Next, we investigated insulin-induced tyrosine phosphorylation of IRS-1, association of PI 3-kinase with IRS-1, and PI 3-kinase activation in skeletal muscle and adipose tissue in vivo by injecting insulin through the portal vein of anaesthetised rats. Protein amount and insulin-induced tyrosine phosphorylation of IRS-1 in skeletal muscle (whole tissue lysates) from BSO-treated rats were similar to those in controls (Fig. 3a, upper panels). Because the insulin signalling in the LDM fraction has been implicated in several insulin actions including insulin-induced glucose uptake [30, 31], we carried out subcellular fractionation studies of skeletal muscles from these rats. Subcellular fractionation data showed insulin-induced tyrosine phosphorylation of IRS-1 in the LDM fraction to be significantly decreased in BSO-treated rats as compared with controls, although the IRS-1 protein amount in this fraction was unchanged (Fig. 3a, upper panels). In the cytosol, the amount of IRS-1 and insulin-induced phosphorylation were similar in BSO-treated and control rat muscles (Fig. 3a, upper panels). Next, we investigated the amount of the p85 subunit for PI 3-kinase protein in whole tissue lysates, the LDM fraction and the cytosol (Fig. 3a, middle panels). The amounts of p85 protein were similar in whole tissue

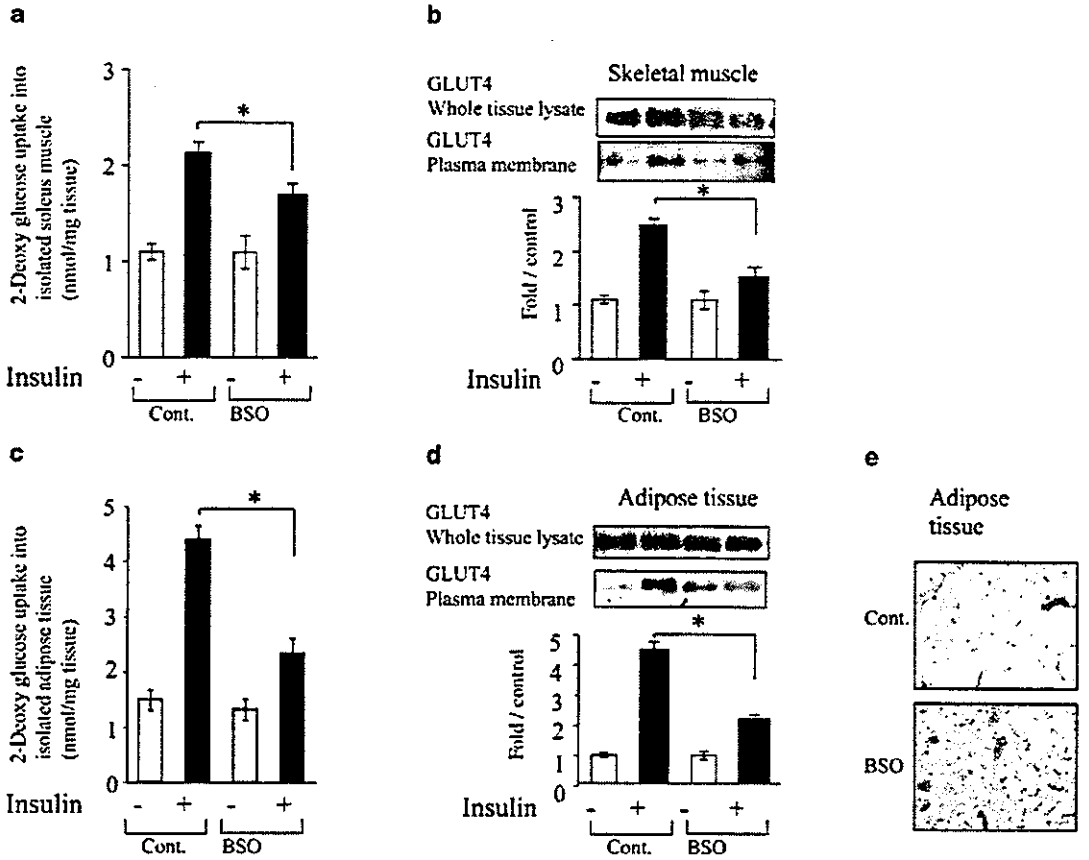

Fig. 2. Insulin resistance in isolated skeletal muscle and adipose tissue in BSO-treated rats. **a.** 2-Deoxy-glucose uptakes into isolated soleus muscle and adipose tissue (**c**). Isolated rat soleus muscle was incubated for 20 min with or without 1.44×10^{-8} mol/l human insulin (this concentration is equivalent to 2 mU/ml) as described previously [17]. 2-Deoxy-D-[1-^{3}H]glucose uptake into the isolated soleus muscle strips was measured as described previously [21]. Isolated rat adipocytes were prepared from epididymal adipose tissue harvested from fasted rats using the collagenase method [22], and 2-deoxy glucose uptake was then assayed as previously described [23]. **b, d.** GLUT4 protein amount in whole tissue lysates (upper panels), the plasma membrane fraction (lower panels) of skeletal muscle (**b**) and adipose tissue (**d**) under basal or insulin-stimulated conditions. Subcellular fractionation and measurement of GLUT4 translocation of isolated skeletal muscle and adipocytes from rats were described previously [12]. Whole tissue lysates and plasma membrane fractions were subjected to SDS-PAGE followed by immunoblotting with anti-GLUT4 antibody. The data are representative of three independent experiments. Bars depict means ± SE of the results from four to six samples. * $p<0.05$ compared with the control under the insulin-stimulated conditions. **d.** Haematoxylin and eosin stained adipose tissues from control and BSO-treated rats are shown. Cont. indicates control Sprague-Dawley rats. BSO indicates rats fed a standard rodent diet with water containing 30 mmol/l BSO for 12 days

lysates before and after insulin stimulation. However, insulin stimulation induced a p85 increase in the LDM fraction and a decrease in the cytosol, suggesting that insulin stimulates p85 translocation from the cytosol to the LDM fraction. This insulin-induced translocation of p85 was disrupted in BSO-treated rats. Insulin-induced increases in IRS-1-associated p85 protein and PI 3-kinase activity did not differ significantly between whole tissue lysates and the cytosol in either BSO-treated or control rat muscle (Fig. 3a, lower panels). However, both were significantly decreased in the LDM fraction of BSO-treated rats as compared with the controls. We obtained essentially the same results in the adipose tissue of these rats (Fig. 3b). In addition, we confirmed that insulin-induced tyrosine phosphorylation of the insulin receptor and IRS-2, as well as Ser-473 phosphorylation of Akt, in the whole tissue lysates of skeletal muscle and adipose tissue does not differ between BSO-treated and control rats (data not shown). Thus, early insulin-signalling steps were shown to be impaired specifically in the LDM fraction, but not in whole tissue lysates of skeletal muscle and adipose tissue from BSO-treated rats.

Insulin action and insulin signalling in BSO-treated 3T3-L1 adipocytes. To further investigate the impaired step in BSO-induced insulin resistance, 3T3-L1

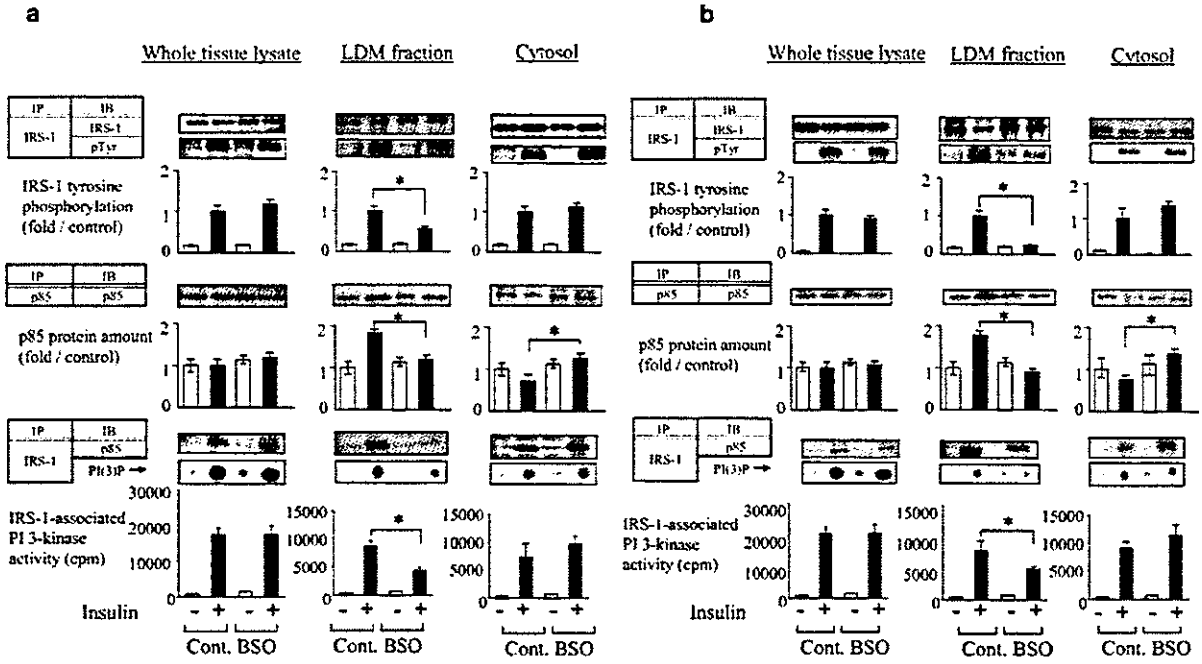

Fig. 3. Insulin signalling in skeletal muscle (**a**) and adipose tissue (**b**) from BSO-treated rats. Rats were anaesthetised, the portal vein exposed, and 16 ml/kg body weight of normal saline, with or without 10^{-5} mol/l human insulin, were injected. After 60 s, hindlimb muscles and epididymal fat were removed and immediately homogenised as described previously [28]. After centrifugation, the resultant supernatants were employed for immunoprecipitation or immunoblotting using the indicated antibodies as described previously [28]. Proteins were visualised with enhanced chemiluminescence and band intensities were quantified with a Molecular Imager GS-525 using Imaging Screen-CH (Bio-Rad). Bars depict means ± SE of the quantitated tyrosine phosphorylation bands, independently obtained in triplicate. Representative spots of PI(3)P are shown in the lower panels and bars depict means ± SE of PI 3-kinase activity measured in three independent assays. * $p<0.05$ compared with the control under the insulin-stimulated condition. IP, immunoprecipitation; IB, immunoblotting; pTyr, phosphotyrosine

adipocytes were incubated with 80 μmol/l BSO for 18 h [32]. It was reported that BSO treatment of adipocytes markedly decreases cellular glutathione levels and increases reactive oxygen species [15, 32]. Incubation with BSO did not affect the morphology or the viability of 3T3-L1 adipocytes (data not shown). Insulin-induced glucose uptake into 3T3-L1 adipocytes was decreased by 42.5% in BSO-treated cells (Fig. 4a). In these cells, insulin-induced GLUT4 translocation to the plasma membrane was impaired (Fig. 4b). Next, we determined insulin-induced IRS-1 phosphorylation and PI 3-kinase activation in whole cell lysates, the LDM fraction and the cytosol. As in rats, protein levels and insulin-induced tyrosine phosphorylations of IRS-1 and IRS-1-associated PI 3-kinase were unaffected by BSO treatment (Fig. 4c, upper panel). In control cells and in BSO-treated cells, p85 protein levels did not differ before versus after insulin stimulation. Next, we examined IRS-1 tyrosine phosphorylation and IRS-1 associated PI 3-kinase activity in the LDM fraction and the cytosol. While IRS-1 protein levels did not change after incubation with BSO, insulin-induced IRS-1 tyrosine phosphorylation in the LDM fraction was suppressed by BSO treatment (Fig. 4c, middle panel). The amount of p85 protein was increased in the LDM fraction and decreased in the cytosol after insulin stimulation, indicating that insulin induces p85 translocation from the cytosol to the LDM fraction in control cells. However, the p85 increase in the LDM fraction was clearly disrupted in BSO-treated cells (Fig. 4c, middle panel). In parallel, insulin-stimulation increased IRS-1-associated p85 protein levels and PI 3-kinase activity in the LDM fraction of control but not BSO-treated cells. Thus, BSO treatment disrupts insulin-induced IRS-1 phosphorylation in the LDM fraction and the subcellular redistribution of PI 3-kinase in 3T3-L1 adipocytes.

Inhibition of NF-κB activation improves BSO-induced insulin resistance. It is widely known that one potential target of oxidative stress is the activation of transcription factor NF-κB [33]. Oxidative stress and inflammatory cytokine stimulation reportedly activate upper kinase IκB kinase (IKK) which phosphorylates serine residues of IκB. The phosphorylated IκB is then subject to degradation, leading to translocation of NF-κB to the nucleus [34]. To investigate the role of NF-κB cascade activation in BSO-induced insulin re-

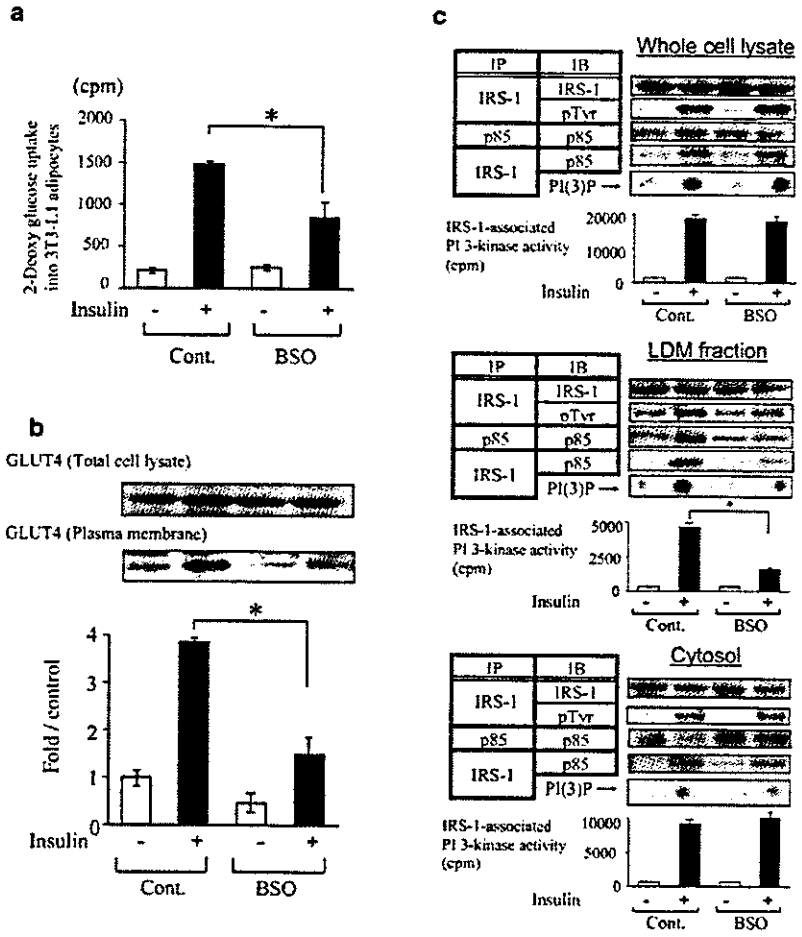

Fig. 4. Effects of BSO treatment on insulin action and insulin signalling in 3T3-L1 adipocytes. **a.** Insulin-induced 2-deoxy glucose uptake into 3T3-L1 adipocytes. 3T3-L1 adipocytes were serum-starved for 18 h, pre-incubated with or without 80 μmol/l BSO for 18 h, then incubated with or without 10^{-6} mol/l insulin for 15 min. 2-Deoxy glucose uptake was measured as described in Materials and methods. Bars depict means ± SE of results obtained independently in triplicate. * $p<0.05$ compared with the insulin-stimulated control. **b.** Recruitment of GLUT4 to the plasma membrane in 3T3-L1 adipocytes with or without BSO pretreatment. 3T3-L1 adipocytes were serum-starved for 18 h, pre-incubated with or without 80 μmol/l BSO for 18 h, then stimulated with or without 10^{-6} mol/l insulin for 15 min. Cells were fractionated as described previously [27]. The cell lysates and plasma membrane fraction were immunoblotted with anti-GLUT4 antibody. Representative immunoblots using anti-GLUT4 antibody are shown. Bars depict means ± SE of the quantitated bands of the plasma membrane fraction, independently obtained in triplicate. **c.** IRS-1 phosphorylation and IRS-1-associated PI 3-kinase in whole cell lysates (upper panels), the LDM fraction (middle panels) and the cytosol (lower panels) in 3T3-L1. 3T3-L1 adipocytes were serum-starved for 18 h, pre-incubated with or without 80 μmol/l BSO for 18 h, then stimulated with or without 10^{-6} mol/l insulin for 15 min. Subcellular fractionation was performed as described in Materials and methods. The whole cell lysates and fractions were used for immunoprecipitation, immunoblotting and PI 3-kinase assay as described previously [28]. Proteins were visualised with enhanced chemiluminescence and band intensities were quantified with a Molecular Imager GS-525. Representative immunoblots are shown in the upper and middle panels and representative spots of PI(3)P, independently obtained in triplicate, are shown in the lower panel. Bars depict means ± SE of the quantitated spots of PI(3)P, indicating IRS-1-associated PI 3-kinase activity, independently obtained in triplicate. Cont., control 3T3-L1 adipocytes; BSO, pre-treated with 80 μmol/l BSO for 18 h. * $p<0.05$ compared with the control under the insulin-stimulated condition

sistance, we overexpressed the dominant negative mutant of IκB in 3T3-L1 adipocytes using adenovirus. This mutant, characterised by the substitution of two serine phosphorylation sites to alanine, is resistant to degradation and inhibits NF-κB-induced transcription. In 3T3-L1 adipocytes, endogenous IκB was degraded by 5.8 pmol/l (equivalent to 10 ng/dl) of TNF-α or 80 μmol/l BSO pre-incubation for 18 h (Fig. 5a). However, the dominant negative IκB, overexpressed using adenovirus, was not degraded by these treat-

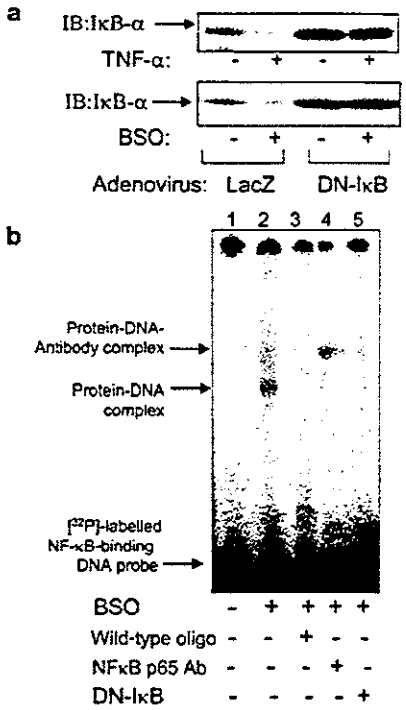

Fig. 5. Dominant negative mutant of IκB. **a.** Immunoblot of 3T3-L1 adipocytes overexpressing LacZ (control) and dominant negative mutant of I-κB adenoviruses. Representative immunoblots with anti-IκBα antibody of the cells incubated with 5.8 pmol/l (equivalent to 10 ng/ml) TNF-α and 80 μmol/l BSO for 18 h are shown in the upper and lower panels respectively. **b.** Gel mobility shift assay (GMSA). 3T3-L1 adipocytes were incubated with (lanes 2–5) or without (lane 1) 80 μmol/l BSO for 18 h. Dominant negative IκB was overexpressed in 3T3-L1 adipocytes (lane 5). Nuclear protein extracts from 3T3-L1 adipocytes were prepared as described in Materials and methods. For the GMSA, 10 μg of nuclear proteins were incubated in binding buffer with 3.5 pmol of double-stranded DNA oligonucleotide containing an NF-κB consensus binding sequence labelled with [^{32}P]-ATP using T4 polynucleotide kinase, for 30 min at 37 °C. For supershift analyses, monoclonal antibody against NF-κB p65 (NF-κB p65 Ab, lane 4) was separately pre-incubated with nuclear extracts at 4 °C for 20 min in a total volume of 16 μl of binding buffer, followed by incubation with 8 μl of ^{32}P-labelled oligonucleotide probe with and without a cold oligonucleotide probe (wild-type oligo, lane 3) at 4 °C for 20 min using a Nushift Kit (Geneka Biotechnology). Protein-DNA complexes were separated from the unbound DNA probe by electrophoresis through 5% polyacrylamide gels containing 1× Tris-glycine-EDTA buffer. The gel was dried and exposed to BAS2000 (Fujifilm, Tokyo, Japan). DN, dominant negative; IB, immunoblotting

ments (Fig. 5a). To investigate whether NF-κB binds to regulatory DNA elements, GMSA was performed using nuclear extracts of 3T3-L1 adipocytes. GMSA revealed nuclear protein extracts from BSO-treated 3T3-L1 adipocytes to contain activated NF-κB (Fig. 5b, lanes 1 and 2). The band shift was inhibited by unlabelled oligonucleotide corresponding to a DNA-binding sequence (Fig. 5b, lane 3). In BSO-treated cells, the NF-κB-oligonucleotide complex underwent a supershift in the presence of antibodies against the p65 subunit of NF-κB, indicating that binding to the oligonucleotide is NF-κB-specific (Fig. 5b, lane 4). In 3T3-L1 adipocytes overexpressing the dominant negative IκB, the band shift was also inhibited (Fig. 5b, lane 5). These results suggest that BSO treatment induces NF-κB translocation and that the dominant negative IκB blocks NF-κB pathway activation.

We next examined the effect of the dominant negative IκB on BSO-induced insulin resistance. Insulin-induced glucose uptake was decreased by BSO treatment, while dominant negative IκB overexpression reversed this decrease (Fig. 6a). Reduction of insulin-induced GLUT4 translocation by BSO administration was also reversed by overexpression of the dominant negative IκB (Fig. 6b). BSO treatment decreased insulin-induced IRS-1 phosphorylation and IRS-1-associated p85 and PI 3-kinase activity in the LDM fraction (Fig. 6c, lower panels), but not in whole cell lysates (Fig. 6c, upper panels). However, overexpression of the dominant negative IκB reversed the BSO-induced decreases in IRS-1 phosphorylation and IRS-1-associated p85 and PI 3-kinase activity in the LDM fraction. These results suggest that oxidative stress induces insulin resistance by impairing the normal subcellular distribution of PI 3-kinase, and that the NF-κB pathway is involved in this process.

Discussion

In this study we employed BSO, a glutathione synthase inhibitor, to induce oxidative stress in rats and in 3T3-L1 adipocytes. BSO specifically inhibits the first step of glutathione synthesis and decreases glutathione, an important component of the antioxidant defence system [14]. In fact, we confirmed a decreased hepatic glutathione content and an increased plasma lipid hydroperoxide level, indicating increased oxidative stress in BSO-treated rats. Body weight was lower in BSO-treated rats than in controls, which is consistent with a previous report [35]. BSO-treated rats were apparently insulin-resistant, as demonstrated by a hyperinsulinaemic-euglycaemic clamp study and glucose transport assay using isolated skeletal muscle and adipocytes. These results strongly support the hypothesis that increased oxidative stress can lead to insulin resistance in vivo. Although fasting insulin levels were not elevated in BSO-treated rats as compared with controls, we found that among well-fed animals, insulin levels were significantly higher in BSO-treated rats than in controls. Data from the euglycaemic-hyperinsulinaemic clamp study, along with the observed glucose uptake into isolated tissues and insulin levels in well-fed animals, support the

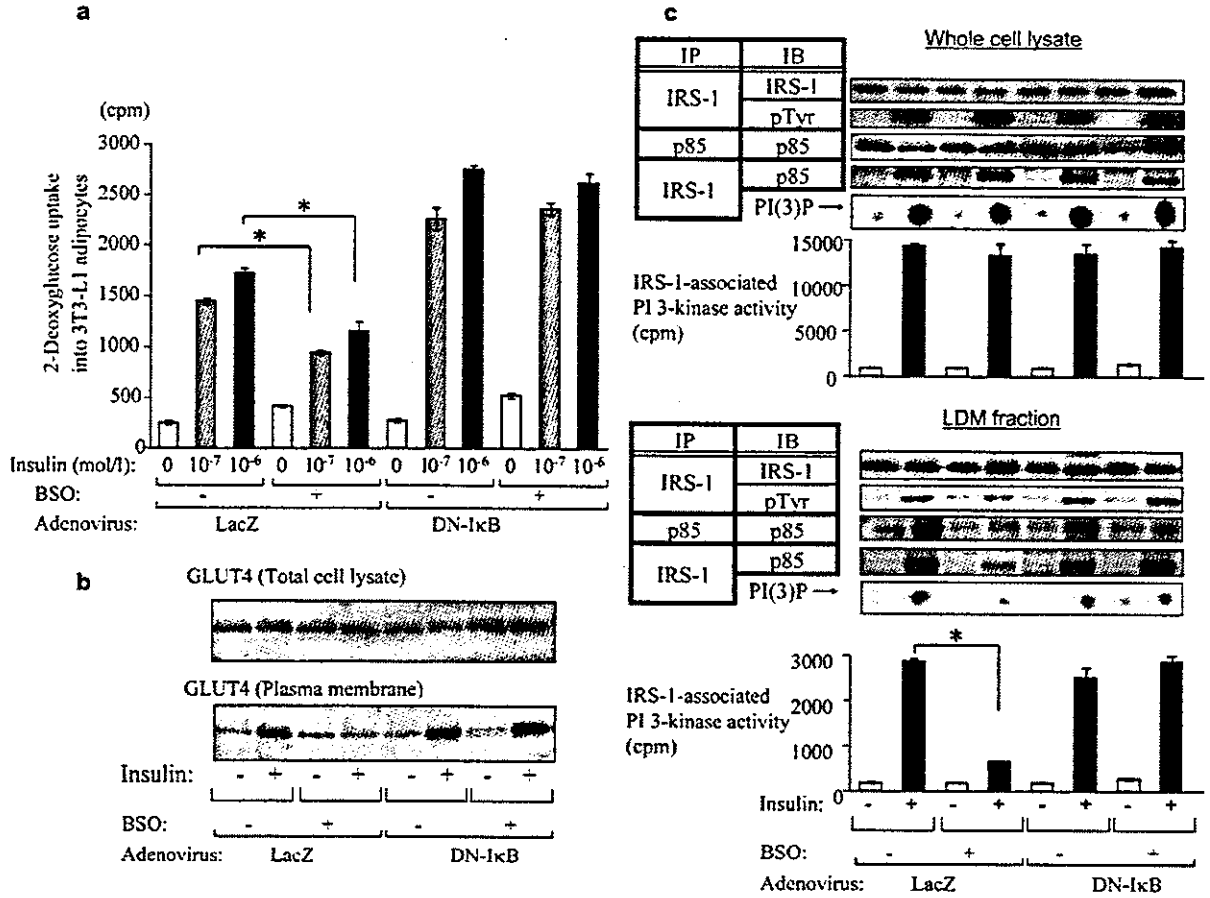

Fig. 6. Effect of dominant negative mutant of IκB on insulin action and insulin signalling in BSO-treated 3T3-L1 adipocytes. **a.** Insulin-induced 2-deoxy glucose uptake into 3T3-L1 adipocytes. Cells overexpressing LacZ (control) and the dominant negative (DN)-IκB adenovirus with or without 80 μmol/l BSO for 18 h were stimulated were stimulated with 0, 10^{-7} or 10^{-6} mol/l insulin for 15 min. Glucose uptake into 3T3-L1 adipocytes was assayed as described in Materials and methods. Bars depict means ± SE of results obtained independently in triplicate. ** $p<0.05$ compared to insulin-stimulated (10^{-7} and 10^{-6} mol/l respectively) control (non BSO-treated) cells. **b.** Recruitment of GLUT4 to the plasma membrane in 3T3-L1 adipocytes overexpressing LacZ and DN-IκB adenovirus with or without BSO pretreatment. The cell lysates and plasma membrane fraction were immunoblotted with anti-GLUT4 antibody. **c.** IRS-1 tyrosine phosphorylation, p85 protein amount and IRS-1-associated PI 3-kinase in whole cell lysates (upper panels) and the LDM fraction (lower panels) of 3T3-L1 adipocytes overexpressing LacZ and DN-IκB adenovirus with or without BSO pretreatment. 3T3-L1 adipocytes were serum-starved for 18 h, pre-incubated with or without 80 μmol/l BSO for 18 h, then stimulated with or without 10^{-6} mol/l insulin for 15 min. Representative immunoblots and representative spots of PI(3)P, independently obtained in triplicate, are shown and bars depict means ± SE of PI 3-kinase activity measured in three independent assays. * $p<0.05$ compared with insulin-stimulated control (non BSO-treated) cells. IB, immunoblotting; IP, immunoprecipitation

conclusion that BSO-treated rats are insulin-resistant. In our experiments, we did not observe the occurrence of overt diabetes with BSO administration, suggesting that this insulin resistance is relatively mild.

A previous report showed no significant difference between BSO-injected rats and controls in terms of insulin-stimulated glucose transport into skeletal muscle [15]. The results of their study contradict our present data demonstrating BSO-induced insulin resistance. We speculate that these different results are attributable to the doses of BSO administered. According to our water consumption data, intake of BSO in BSO-treated rats was approximately 3.5 mmol·kg^{-1} body weight·day^{-1} in the current study. This is a rather high dose compared with the previous report (2 mmol·kg^{-1} body weight·day^{-1}) [15]. Also, the extent of the glutathione decrease was greater in our experiment than in the previous one. In addition, because the previous study did not employ the hyperinsulinaemic-euglycaemic clamp method [15], we believe our picture of insulin resistance in BSO-treated rats to be more accurate.

Insulin-induced IRS phosphorylation and PI 3-kinase activation constitute a critical step in insulin actions such as GLUT4 translocation and glucose uptake [36]. Most insulin-resistant models have been shown

to have impaired insulin-induced PI 3-kinase activation [28, 37, 38]. However, in the BSO-treated rats used in the current study, neither insulin-induced IRS tyrosine phosphorylation nor PI 3-kinase activation in whole tissue lysates of skeletal muscle and adipose tissue were impaired, despite the presence of insulin resistance. In addition, BSO treatment markedly impaired insulin-induced glucose uptake into 3T3-L1 adipocytes and GLUT4 translocation, while insulin-induced IRS-1 tyrosine phosphorylation and IRS-1-associated PI 3-kinase activation were unchanged in whole cell lysates of BSO-treated 3T3-L1 adipocytes. A previous report showed H_2O_2 exposure of 3T3-L1 adipocytes to inhibit insulin-induced glucose uptake, while having no effects on IRS-1 phosphorylation and PI 3-kinase activation [39]. Furthermore, we previously reported chronically angiotensin-II-infused rats, in which plasma lipid hydroperoxide levels were increased, to be highly insulin-resistant, although insulin-induced IRS-1 phosphorylation and PI 3-kinase activation in skeletal muscle and adipose tissue were not impaired [12]. Thus, insulin resistance with normal insulin-induced PI 3-kinase activation in the whole cell may be a common feature in the models with increased oxidative stress.

Regarding the molecular mechanism of this type of insulin resistance, we consider it necessary to examine the possibility of abnormalities in the subcellular distribution of PI 3-kinase. This is based on several reports showing IRS-1 phosphorylation and PI 3-kinase activation specifically in the LDM fraction, though not in whole cell lysates, to be important for insulin action [30, 31]. We speculate that the insulin-induced increase in IRS-1 phosphorylation in the LDM fraction leads to recruitment of the p85 subunit for PI 3-kinase to that fraction. Previous reports have shown that H_2O_2 exposure reduces IRS-1 tyrosine phosphorylation and PI 3-kinase activation in the LDM fraction in 3T3-L1 adipocytes [39, 40]. In the current study, insulin-induced IRS-1 tyrosine phosphorylation in the LDM fraction was demonstrated to be significantly decreased in both BSO-treated rat muscle and adipose tissues and in BSO-treated 3T3-L1 cells. We showed clearly that insulin induces p85 translocation from the cytosol to the LDM fraction in rat muscle, adipose tissue and 3T3-L1 cells and that BSO treatment disrupts this process. Taking our results and those of previous reports together, we consider this disruption of the normal subcellular redistribution of PI 3-kinase to be one of the important mechanisms underlying oxidative-stress-induced insulin resistance.

The activation of transcription factor NF-κB has been shown to be a target of oxidative stress [33]. For example, direct exposure to oxidants such as H_2O_2 activates NF-κB [41], while NF-κB activation can be inhibited by addition of antioxidants such as a vitamin E derivative [42] and lipoic acid [43]. To clarify the contribution of NF-κB cascade activation to oxidative-stress-induced insulin resistance, we utilised the dominant negative IκB. This mutant is a degradation-resistant form of IκB that prevents NF-κB from translocating into the nucleus and is widely used to block cytokine-induced NF-κB activation [44]. Indeed, we confirmed that this mutant is not degraded by TNF-α and that BSO stimulation blocks NF-κB from translocating into the nucleus. Blocking the NF-κB cascade by overexpressing dominant negative IκB had a preventive effect against the decrease in insulin-induced glucose uptake and GLUT4 translocation caused by BSO treatment in 3T3-L1 adipocytes. We observed higher glucose uptake in dominant negative IκB-overexpressing cells than in LacZ control cells. We suggest a possible explanation: dominant negative IκB inhibits the effects of a small amount of inflammatory cytokines secreted by adipocytes. In addition, BSO-induced decreases in IRS-1 tyrosine phosphorylation in the LDM fraction and recruitment of PI 3-kinase to that fraction were also normalised. These results suggest that NF-κB activation is involved in the impaired subcellular redistribution of PI 3-kinase and the insulin resistance induced by BSO treatment.

The precise mechanism linking NF-κB activation and abnormal subcellular redistribution of PI 3-kinase remains unclear. One possible mechanism of inhibited insulin signalling involves NF-κB-activated transcription of inflammatory cytokines such as TNF-α and interleukin-6. NF-κB plays an important role in regulating inflammatory responses [45, 46] and activation of NF-κB may induce inappropriate inflammatory responses, possibly disrupting insulin signalling. Alternatively, PI 3-kinase activation is reportedly necessary for NF-κB activation [47, 48]. Aberrant NF-κB activation may disrupt the PI 3-kinase pathway via a negative feedback mechanism. An anti-inflammatory agent, salicylate, which stabilises IκB via inhibition of IKK and suppression of NF-κB activation, was shown to restore lipid-induced insulin resistance [49, 50]. Because IKK reportedly induces serine phosphorylation of IRS-1, it is possible that BSO activates IKK, resulting in down-regulation of IRS-1 tyrosine phosphorylation in the LDM fraction and impairment of PI 3-kinase recruitment to the LDM fraction.

In summary, our results suggest that oxidative stress induces insulin resistance by impairing insulin-induced IRS-1 phosphorylation in the LDM fraction and subcellular redistribution of PI 3-kinase, and that NF-κB activation is involved in this process. Our present study provides evidence that the NF-κB pathway plays a role in the pathogenesis of oxidative-stress-induced insulin resistance. Judging from our results and those of previous studies, strategies designed to limit inappropriate activation of NF-κB may be an effective approach to treating insulin resistance.

Acknowledgements. The dominant negative mutant of IκB was kindly provided by Dr Richard Gaynor (University of Texas Southwestern Medical Center at Dallas, Tex., USA). The authors are indebted to Naomasa Kakiya of the University of Tokyo for assistance in various areas of this study.

References

1. Betteridge DJ (2000) What is oxidative stress? Metabolism 49 [Suppl 1]:3–8
2. Reaven GM, Lithell H, Landsberg L (1996) Hypertension and associated metabolic abnormalities—the role of insulin resistance and the sympathoadrenal system. N Engl J Med 334:374–381
3. Tuck ML (1990) Metabolic considerations in hypertension. Am J Hypertens 3:355S–365S
4. Baynes JW (1991) Role of oxidative stress in development of complications in diabetes. Diabetes 40:405–412
5. Paolisso G, D'Amore A, Volpe C et al. (1994) Evidence for a relationship between oxidative stress and insulin action in non-insulin-dependent (type II) diabetic patients. Metabolism 43:1426–1429
6. Jones AF, Winkles JW, Jennings PE et al. (1988) Serum antioxidant activity in diabetes mellitus. Diabetes Res 7:89–92
7. Paolisso G, Di Maro G, Pizza G et al. (1992) Plasma GSH/GSSG affects glucose homeostasis in healthy subjects and non-insulin-dependent diabetics. Am J Physiol 263:E435–E440
8. Paolisso G, Balbi V, Volpe C et al. (1995) Metabolic benefits deriving from chronic vitamin C supplementation in aged non-insulin dependent diabetics. J Am Coll Nutr 14:387–392
9. Paolisso G, Di Maro G, Galzerano D et al. (1994) Pharmacological doses of vitamin E and insulin action in elderly subjects. Am J Clin Nutr 59:1291–1296
10. Rajagopalan S, Kurz S, Munzel T et al. (1996) Angiotensin II-mediated hypertension in the rat increases vascular superoxide production via membrane NADH/NADPH oxidase activation. Contribution to alterations of vasomotor tone. J Clin Invest 97:1916–1923
11. Schnackenberg CG, Wilcox CS (1999) Two-week administration of tempol attenuates both hypertension and renal excretion of 8-Iso prostaglandin f2alpha. Hypertension 33:424–428
12. Ogihara T, Asano T, Ando K et al. (2002) Angiotensin II-induced insulin resistance is associated with enhanced insulin signalling. Hypertension 40:872–879
13. Shimosawa T, Ogihara T, Matsui H et al. (2003) Deficiency of adrenomedullin induces insulin resistance by increasing oxidative stress. Hypertension 41:1080–1085
14. Meister A (1983) Selective modification of glutathione metabolism. Science 220:472–477
15. Khamaisi M, Kavel O, Rosenstock M et al. (2000) Effect of inhibition of glutathione synthesis on insulin action: in vivo and in vitro studies using buthionine sulfoximine. Biochem J 349:579–586
16. Vaziri ND, Wang XQ, Oveisi F, Rad B (2000) Induction of oxidative stress by glutathione depletion causes severe hypertension in normal rats. Hypertension 36:142–146
17. Ogihara T, Asano T, Ando K et al. (2001) Insulin resistance with enhanced insulin signalling in high-salt diet-fed rats. Diabetes 50:573–583
18. Yamamoto Y (1994) Chemiluminescence-based high-performance liquid chromatography assay of lipid hydroperoxides. Methods Enzymol 233:319–324
19. Anderson ME (1985) Determination of glutathione and glutathione disulfide in biological samples. Methods Enzymol 113:548–555
20. James DE, Burleigh KM, Kraegen EW (1986) In vivo glucose metabolism in individual tissues of the rat. Interaction between epinephrine and insulin. J Biol Chem 261:6366–6374
21. Hansen P, Gulve EA, Holloszy JO (1994) Suitability of 2-deoxyglucose for in vitro measurement of glucose transport activity in skeletal muscle. J Appl Physiol 76:979–985
22. Rodbell M (1964) Metabolism of isolated fat cells. I. Effects of hormones on glucose metabolism and lipolysis. J Biol Chem 239:375–380
23. Olefsky JM (1975) Effect of dexamethasone on insulin binding, glucose transport, and glucose oxidation of isolated rat adipocytes. J Clin Invest 56:1499–1508
24. Fujishiro M, Gotoh Y, Katagiri H et al. (2001) MKK6/3 and p38 MAPK pathway activation is not necessary for insulin-induced glucose uptake but regulates glucose transporter expression. J Biol Chem 276:19800–19806
25. Katagiri H, Asano T, Ishihara H et al. (1996) Overexpression of catalytic subunit p110alpha of phosphatidylinositol 3-kinase increases glucose transport activity with translocation of glucose transporters in 3T3-L1 adipocytes. J Biol Chem 271:16987–16990
26. Asano T, Kanda A, Katagiri H et al. (2000) p110beta is up-regulated during differentiation of 3T3-L1 cells and contributes to the highly insulin-responsive glucose transport activity. J Biol Chem 275:17671–17676
27. Satoh S, Nishimura H, Clark AE et al. (1993) Use of bismannose photolabel to elucidate insulin-regulated GLUT4 subcellular trafficking kinetics in rat adipose cells. Evidence that exocytosis is a critical site of hormone action. J Biol Chem 268:17820–17829
28. Anai M, Funaki M, Ogihara T et al. (1998) Altered expression levels and impaired steps in the pathway to phosphatidylinositol 3-kinase activation via insulin receptor substrates 1 and 2 in Zucker fatty rats. Diabetes 47:13–23
29. Sakoda H, Ogihara T, Anai M et al. (1999) No correlation of plasma cell 1 overexpression with insulin resistance in diabetic rats and 3T3-L1 adipocytes. Diabetes 48:1365–1371
30. Anai M, Ono H, Funaki M et al. (1998) Different subcellular distribution and regulation of expression of insulin receptor substrate (IRS)-3 from those of IRS-1 and IRS-2. J Biol Chem 273:29686–29692
31. Kriauciunas KM, Myers MG Jr, Kahn CR (2000) Cellular compartmentalization in insulin action: altered signaling by a lipid-modified IRS-1. Mol Cell Biol 20:6849–6859
32. Lu B, Ennis D, Lai R et al. (2001) Enhanced sensitivity of insulin-resistant adipocytes to vanadate is associated with oxidative stress and decreased reduction of vanadate (+5) to vanadyl (+4). J Biol Chem 276:35589–35598
33. Schreck R, Albermann K, Baeuerle PA (1992) Nuclear factor kappa B: an oxidative stress-responsive transcription factor of eukaryotic cells (a review). Free Radic Res Commun 17:221–237
34. Siebenlist U, Franzoso G, Brown K (1994) Structure, regulation and function of NF-kappa B. Annu Rev Cell Biol 10:405–455
35. Leeuwenburgh C, Ji LL (1995) Glutathione depletion in rested and exercised mice: biochemical consequence and adaptation. Arch Biochem Biophys 316:941–949
36. Czech MP (1995) Molecular actions of insulin on glucose transport. Annu Rev Nutr 15:441–471

37. Saad MJ, Folli F, Kahn JA, Kahn CR (1993) Modulation of insulin receptor, insulin receptor substrate-1, and phosphatidylinositol 3-kinase in liver and muscle of dexamethasone-treated rats. J Clin Invest 92:2065–2072
38. Cusi K, Maezono K, Osman A et al. (2000) Insulin resistance differentially affects the PI 3-kinase- and MAP kinase-mediated signalling in human muscle. J Clin Invest 105:311–320
39. Rudich A, Tirosh A, Potashnik R, Hemi R, Kanety H, Bashan N (1998) Prolonged oxidative stress impairs insulin-induced GLUT4 translocation in 3T3-L1 adipocytes. Diabetes 47:1562–1569
40. Tirosh A, Potashnik R, Bashan N, Rudich A (1999) Oxidative stress disrupts insulin-induced cellular redistribution of insulin receptor substrate-1 and phosphatidylinositol 3-kinase in 3T3-L1 adipocytes. A putative cellular mechanism for impaired protein kinase B activation and GLUT4 translocation. J Biol Chem 274:10595–10602
41. Schreck R, Rieber P, Baeuerle PA (1991) Reactive oxygen intermediates as apparently widely used messengers in the activation of the NF-kappa B transcription factor and HIV-1. EMBO J 10:2247–2258
42. Suzuki YJ, Packer L (1993) Inhibition of NF-kappa B activation by vitamin E derivatives. Biochem Biophys Res Commun 193:277–283
43. Sen CK, Packer L (1996) Antioxidant and redox regulation of gene transcription. FASEB J 10:709–720
44. Yamamoto Y, Gaynor RB (2001) Therapeutic potential of inhibition of the NF-kappaB pathway in the treatment of inflammation and cancer. J Clin Invest 107:135–142
45. Baeuerle PA, Henkel T (1994) Function and activation of NF-kappa B in the immune system. Annu Rev Immunol 12:141–179
46. Barnes PJ, Karin M (1997) Nuclear factor-kappaB: a pivotal transcription factor in chronic inflammatory diseases. N Engl J Med 336:1066–1071
47. Sizemore N, Leung S, Stark GR (1999) Activation of phosphatidylinositol 3-kinase in response to interleukin-1 leads to phosphorylation and activation of the NF-kappaB p65/RelA subunit. Mol Cell Biol 19:4798–4805
48. Reddy SA, Huang JH, Liao WS (2000) Phosphatidylinositol 3-kinase as a mediator of TNF-induced NF-kappa B activation. J Immunol 164:1355–1363
49. Kim JK, Kim YJ, Fillmore JJ et al. (2001) Prevention of fat-induced insulin resistance by salicylate. J Clin Invest 108:437–446
50. Yuan M, Konstantopoulos N, Lee J et al. (2001) Reversal of obesity- and diet-induced insulin resistance with salicylates or targeted disruption of Ikkbeta. Science 293:1673–1677

Available online at www.sciencedirect.com
SCIENCE DIRECT
Journal of Molecular and Cellular Cardiology 36 (2004) 175–183
Journal of Molecular and Cellular Cardiology
www.elsevier.com/locate/yjmcc

Review Article

Vascular cell senescence and vascular aging☆

Tohru Minamino, Hideyuki Miyauchi, Toshihiko Yoshida, Kaoru Tateno, Takeshige Kunieda, Issei Komuro *

Department of Cardiovascular Science and Medicine, Chiba University Graduate School of Medicine, 1-8-1 Inohana, Chuo-ku, Chiba 260-8670, Japan

Received 20 August 2003; received in revised form 15 November 2003; accepted 17 November 2003

Abstract

Vascular cells have a finite lifespan when cultured in vitro and eventually enter an irreversible growth arrest called "cellular senescence". A number of genetic animal models carrying targeted disruption of the genes that confer the protection against senescence in vitro have been reported to exhibit the phenotypes of premature aging. Similar mutations have been found in the patients with premature aging syndromes. Many of the changes in senescent vascular cell behavior are consistent with the changes seen in age-related vascular diseases. We have demonstrated the presence of senescent vascular cells in human atherosclerotic lesions but not in non-atherosclerotic lesions. Moreover, these cells express increased levels of pro-inflammatory molecules and decreased levels of endothelial nitric oxide synthase, suggesting that cellular senescence in vivo contributes to the pathogenesis of human atherosclerosis. One widely discussed hypothesis of senescence is the telomere hypothesis. An increasing body of evidence has established the critical role of the telomere in vascular cell senescence. Another line of evidence suggests that telomere-independent mechanisms are also involved in vascular cell senescence. Activation of Ras, an important signaling molecule involved in atherogenic stimuli, induces vascular cell senescence and thereby promotes vascular inflammation in vitro and in vivo. It is possible that mitogenic-signaling pathways induce telomere-dependent and telomere-independent senescence, which results in vascular dysfunction. Further understanding of the mechanism underlying cellular senescence will provide insights into the potential of antisenescence therapy for vascular aging.

© 2003 Elsevier Ltd. All rights reserved.

Keywords: Senescence; Aging; Atherosclerosis; Telomere; Ras; Akt; Inflammation; Cyclin-dependent kinase inhibitor

1. Introduction

Cellular senescence is the limited ability of primary human cells to divide when cultured in vitro and is accompanied by a specific set of phenotypic changes in morphology, gene expression and function. These changes in phenotype have been implicated in human aging [1]. This hypothesis, the hypothesis of cellular aging, was first described by Hayflick [2] and supported by evidence that cellular senescence and the division potential of human primary cultures are dependent on donor age [3] and that the growth potential of cultures correlates well with mean maximum lifespan of the species from which the cultures are derived [4]. Human primary cultures derived from the patients with premature aging syndromes, such as Werner syndrome and Bloom syndrome, are known to have shorter lifespan than the cultures from age-matched healthy populations [5], thus supporting the hypothesis of aging. However, until recently, little attention has been paid on the potential impact of vascular cell senescence in vivo on age-related vascular disorders.

In the past decades, significant progress has been made in our understanding of the mechanisms underlying cellular senescence. One widely discussed hypothesis is the telomere hypothesis of senescence [6]. A growing body of evidence has demonstrated a critical role of telomere and telomerase in regulating not only cellular lifespan but also organismal aging. However, recent findings suggest that cellular senescence can also be induced by DNA damage, cellular stress or oncogenic activation, which is independent of replicative age [7]. For example, the constitutive activation of mitogenic stimuli by expression of oncogenic Ras induces senescent phenotypes [8–10]. Thus, it is possible that atherogenic stimuli increase cell turnover at the sites of atherosclerosis, thereby promoting telomere shortening, whereas it also re-

☆ The review process for this manuscript was handled by Consulting Editor, Eduardo Marban.

* Corresponding author. Tel.: +81-43-226-2097; fax: +81-43-226-2557
E-mail address: komuro-tky@umin.ac.jp (I. Komuro).

© 2003 Elsevier Ltd. All rights reserved.
doi:10.1016/j.yjmcc.2003.11.010